Article

Spectroelectrochemical Study of the Photoinduced Catalytic Formation of 4,4'-Dimercaptoazobenzene from 4-Aminobenzenethiol Adsorbed on Nanostructured Copper

Francisco J. Vidal-Iglesias, Jose Solla-Gullon, Jose Manuel Orts, Antonio Rodes, and Juan Manuel Pérez

J. Phys. Chem. C, **Just Accepted Manuscript** • DOI: 10.1021/acs.jpcc.5b01245 • Publication Date (Web): 12 May 2015

Spectroelectrochemical Study of the Photoinduced Catalytic Formation of 4,4'-Dimercaptoazobenzene from 4-Aminobenzenethiol Adsorbed on Nanostructured Copper

Francisco J. Vidal-Iglesias[b], *Jose Solla-Gullon*[b], *Jose M. Orts*[a,b], *Antonio Rodes*[a,b] *and Juan M. Perez*[a,b]*

[a] Departamento de Química Física, Universidad de Alicante, E-03080 Alicante, Spain

[b] Instituto Universitario de Electroquímica, Universidad de Alicante, E-03080 Alicante, Spain.

ABSTRACT

Surface-Enhanced Raman Scattering (SERS) spectra of self-assembled monolayers of 4-aminobenzenethiol (4-ABT) on copper (Cu) and silver (Ag) surfaces decorated with Cu and Ag nanostructures, respectively, have been obtained with lasers at 532 nm, 632.8 nm, 785 nm and 1064 nm. Density Functional Theory (DFT) has been used to obtain calculated vibrational frequencies of the 4-ABT and 4,4'-dimercaptoazobenzene (4,4'-DMAB) molecules adsorbed on model Cu surfaces. The features of the SERS spectra depend on the electrode potential and the

type and power density of the laser. SERS spectra showed the formation of the 4,4'-DMAB on the nanostructured Cu surface independently of the laser employed. For the sake of comparison SERS spectra of a self-assembled monolayer of the 4-ABT on Ag surfaces decorated with Ag nanostructures have been also obtained with the same four lasers. When using the 532 nm and 632.8 nm lasers, the 4,4'-DMAB is formed on Cu surface at electrode potentials as low as -1.0 V (AgCl/Ag) showing a different behaviour with respect to Ag (and others metals such as Au and Pt). On the other hand, the Surface-Enhanced Infrared Reflection Absorption (SEIRA) spectra showed that in absence of the laser excitation the 4,4'-DMAB is not produced from the adsorbed 4-ABT on nanostructured Cu in the whole range of potentials studied. These results point out the prevalence of the role of electron-hole pairs through surface plasmon activity to explain the obtained SERS spectra.

INTRODUCTION

Raman scattering of adsorbed molecules on nanostructured metal surfaces can benefit from a very large increase in sensitivity. Surface-Enhanced Raman Scattering (SERS) was first observed in 1974 [1] and since then, it has attracted substantial interest owing to its great potential in many fields (analytical, technology and research). Noble metal nanostructures exhibit SERS, the scattering cross sections of which are dramatically enhanced for molecules adsorbed thereon.[2] Since its discovery SERS [1, 3] has been studied extensively, both experimentally and theoretically [4-7] because of its extremely high surface sensitivity and powerful application on fingerprint vibrational spectroscopy in qualitative and quantitative analysis, even at the single-molecule

level. It is generally accepted that two different mechanisms are involved in SERS: electromagnetic (EM) [8-10] and chemical enhancement (CE).[11-13]

Further insight on the bonding and interactions between adsorbates can be gained by complementing the vibrational information provided by SERS with that derived from infrared spectroscopy experiments. In this way, Surface Enhanced Infrared Reflection Absorption Spectroscopy (SEIRAS) under attenuated total reflection conditions (ATR) is now a well established technique for the in-situ characterization of adsorption/desorption and reaction processes at the electrode/solution interphase.[14-15] When compared with the external-reflection approach used in InfraRed Reflection Absorption Spectroscopy (IRRAS) experiments, the use of deposited metal thin-film electrodes (in the so-called Kretschmann's configuration) provides a selective enhancement of the infrared absorption for adsorbates that allows increased sensitivity, better conditions for the study of water-metal and water-adsorbate interactions as well as the possibility of kinetic experiments in the submillisecond range.[14-17] Similarly to the SERS effect, the SEIRA effect has been related to the nanostructure of thin film and explained as a result of an enhancement of the electric field at the surface of the grains forming the metal thin film. [14, 18]

Aminobenzenethiols (ABT) are frequently studied as SERS probe molecules [19-20] and particularly 4-ABT is widely used as molecular junction [21-22] and building block in SAMs.[21] Extensive experimental studies have been performed on the SERS of 4-aminobenzenethiol adsorbed on different metal surfaces, including transition metals such as Pt [23] and in metal-molecule-metal junction systems.[20-31] The SERS from the self-assembled monolayer of 4-ABT on Ag and Au is significantly different from the normal Raman spectrum of the molecule in solid state. In normal Raman spectrum only bands that correspond to completely symmetric a_1 vibrations are observed, whereas in its SERS spectrum, non-a_1-type bands (appearing at 1142

cm^{-1}, 1390 cm^{-1} and 1432 cm^{-1}) are also present under open circuit conditions [20, 28] or when applying high enough electrode potentials.[24, 32] However, SERS spectra from benzenethiol on these metals are substantially similar to those obtained from the normal Raman spectrum. The enhancement mechanism for the three non-a_1-type strongly enhanced Raman peaks at 1142, 1390, and 1432 cm^{-1} was first interpreted as a case of chemical enhancement by Osawa et al. in 1994.[28] It was speculated [24, 28] that the alteration of the spectrum of 4-ABT could be due to the contribution of the CT mechanism in enhancement, as a consequence of the alteration of electronic states of benzenethiol by the introduction of an NH_2 group in the benzene ring. Since then, many papers have been published, and the three strongly enhanced Raman peaks have been widely considered as an experimental evidence of a chemical mechanism of SERS.[20-21, 28-31] Alternatively, it has been also proposed, based on the spectral similarity of 4-ABT and 4,4'-dimercaptoazobenzene (4,4'-DMAB) adsorbed on Ag, that these bands correspond to N=N stretching (a_g symmetric vibrational modes) of 4,4'-DMAB produced from 4-ABT via a photocatalytic coupling reaction.[24, 32] Recently, similar SERS spectra have been obtained when 4-ABT was adsorbed on nanostructured Pt substrates.[23] These spectra showed bands not observed in the normal Raman spectrum of 4-ABT, both under open circuit conditions and when applying electrode potentials above -0.50 V (vs. AgCl/Ag), which disappear when the electrode potential is shifted to more negative values. Bands attributed to the formation of 4,4'-DMAB have been also observed in SERS of 4-ABT adsorbed onto assemblies of Au-Cu core-shell nanoparticles, as in the cases of Ag, Au and Pt surfaces, by using a 632.8 nm laser.[33] In addition, Sun et al.[27] have found that with Cu colloids, 4,4'-DMAB can be produced from 4-ABT by a surface-catalyzed reaction. These experimental results are strongly supported by Wu's theoretical work.[26] Recently, Wu et al. have also investigated the electrooxidation of 4-ABT on gold

electrodes by means of density functional theory (DFT) providing mechanistic insight into this reaction at metal electrodes.[34] On the other hand, Dendisova-Vyskovska et al.[35] have used the spectra of adsorbed 4-ABT to evaluate the effectiveness of SERS on different Cu substrates at 1064-nm excitation using a FT-Raman spectrometer. However, no evidence of formation of 4,4′-DMAB was found under these experimental conditions as indicated by the absence of bands around 1142, 1390, and 1432 cm^{-1}. Recently, Matejka et al.[36] have reported that in the case of Cu surfaces activated by electrochemical methods (oxidation-reduction cycling) and excited by a diode laser of 785 nm, only characteristic bands of 4-ABT are observed in the whole potential range. According with these results, they concluded that the nature of the metal could also play an important role in the formation of the azobenzene derivative.

In this work we study whether the role of Cu regarding the eventual formation of 4,4'-DMAB from adsorbed 4-ABT is really different from those observed with Ag, Au and Pt. To do this, we have performed DFT calculations to obtain the vibrational frequencies of the 4-ABT molecule, in gas phase and adsorbed on Cu surfaces, as well as those of the 4,4'-DMAB. We also study by SEIRA spectroscopy, for the first time, whether new species can be formed from the adsorbed 4-ABT when the potential of the copper electrode is modified in the absence of laser excitation. Next, we have recorded SERS spectra of adsorbed 4-ABT on a Cu electrode decorated with Cu nanostructures using four different lasers (532 nm 632.8 nm, 785 nm and 1064 nm) as excitation sources. These spectra have been compared with those obtained with the same lasers from a Ag electrode decorated with Ag nanostructures using similar experimental conditions. In addition, SERS spectra of 4,4'-DMAB on nanostructured Cu electrodes have been also recorded. As it will be shown below, the set of SERS spectra obtained shows that Cu is not an exception in producing 4,4'-DMAB from the adsorbed 4-ABT. These findings also support the formation of

4,4'-DMAB on Cu surfaces from 4-ABT with lasers of wavelengths longer than 700 nm. Consequently, the prevalence of the role of electron-hole pairs through surface plasmon activity is invoked to explain the SERS spectra obtained.

EXPERIMENTAL AND COMPUTATIONAL DETAILS

Electrochemical measurements. Electrochemical measurements were performed in 0.1 M $NaClO_4$ (Fluka, ≥98.0%) or in 0.1 M $NaClO_4$ + 10^{-3} M 4-ABT (Aldrich, 97%) solutions at room temperature. For the electrochemical study in presence of 4,4'-DMAB (prepared by Tian's group [24]), the electrode was initially immersed in an ethanolic solution containing the 4,4'-DMAB (saturated solution diluted 10 times) for at least 5 minutes and then transferred into an electrochemical cell containing a 0.1 M $NaClO_4$ solution and immersed at a controlled potential of 0 V. Working solutions were daily prepared using Millipore Milli-Q water (18.2 MΩ·cm) and solutions were deaerated with Ar (N50, Air Liquide). A three-electrode electrochemical cell was used. The electrode potential was controlled using a PGSTAT302N AUTOLAB system. The counter electrode was a polished Au wire and the working electrode was a polyoriented Cu rod or a flame annealed Ag bead electrode. Potentials were measured against an AgCl/Ag reference electrode (CH Instruments, Inc.) connected to the cell through a Luggin capillary.

Synthesis of nanostructures. The synthesis of the Cu and Ag nanostructures was performed using a methodology similar to that described in previous contributions [37-39] for the synthesis of Pt and Au nanoparticles. In brief, 20 mL of an aqueous solution of the metallic precursor containing 2.5×10^{-4} M $Cu(NO_3)_2$ (Aldrich, 99.999%) or 2.5×10^{-4} M $AgNO_3$ (Panreac, 99%) and 2.5×10^{-4} M trisodium citrate (Sigma-Aldrich, ≥99.0%) was prepared in a glass beaker at room temperature. Then, 0.6 mL of an ice-cold and freshly prepared 0.1 M $NaBH_4$ (Aldrich,

99%) solution was added to the solution under vigorous stirring. The stirring was slowed down after 30 s and the solution was keep unperturbed for the next 30 min. Once the nanostructures were synthesized, it was necessary a cleaning protocol to remove the capping agent, citrate in this particular case, attached to the surface of the nanostructures. Following previous findings,[37-38] it could be achieved by the direct addition of a NaOH (Merck, p.a.) pellet (≈ 0.2 g) to each colloidal solution. This addition of NaOH produces the destabilization of the colloid giving rise to the precipitation of the nanostructures. After complete precipitation, the sample was washed 3–4 times with ultrapure water. TEM experiments were performed with a JEOL, JEM 2010 microscope working at 200 kV. The sample for TEM analysis was obtained by placing a drop of the water suspension containing the clean nanostructures onto a Formvar-covered copper grid and evaporating the solvent in air at room temperature. Figure 1 shows some representative TEM images of the (A) Ag and (B) Cu obtained nanostructures. As previously mentioned, the use of surface cleaned (organics free) nanostructures is a relevant aspect for studying electro-catalytic surface reactions. However, as recently described with similar Ag nanostructures,[40] the removal of the capping agent protecting the Ag (about 6 nm) nanoparticles results in a higher degree of agglomeration (contact between different nanoparticles) and in a certain degree of coalescence (mainly through Ostwald ripening) which induces not only a growth of the nanoparticles but also the formation of nanochains between them as also illustrated in figure 1A. In the case of Cu, the TEM image obtained with the NaOH-treated Cu sample clearly shows that the Cu material is not formed by nanoparticles but by agglomerated nanoneedles (figure 1B).

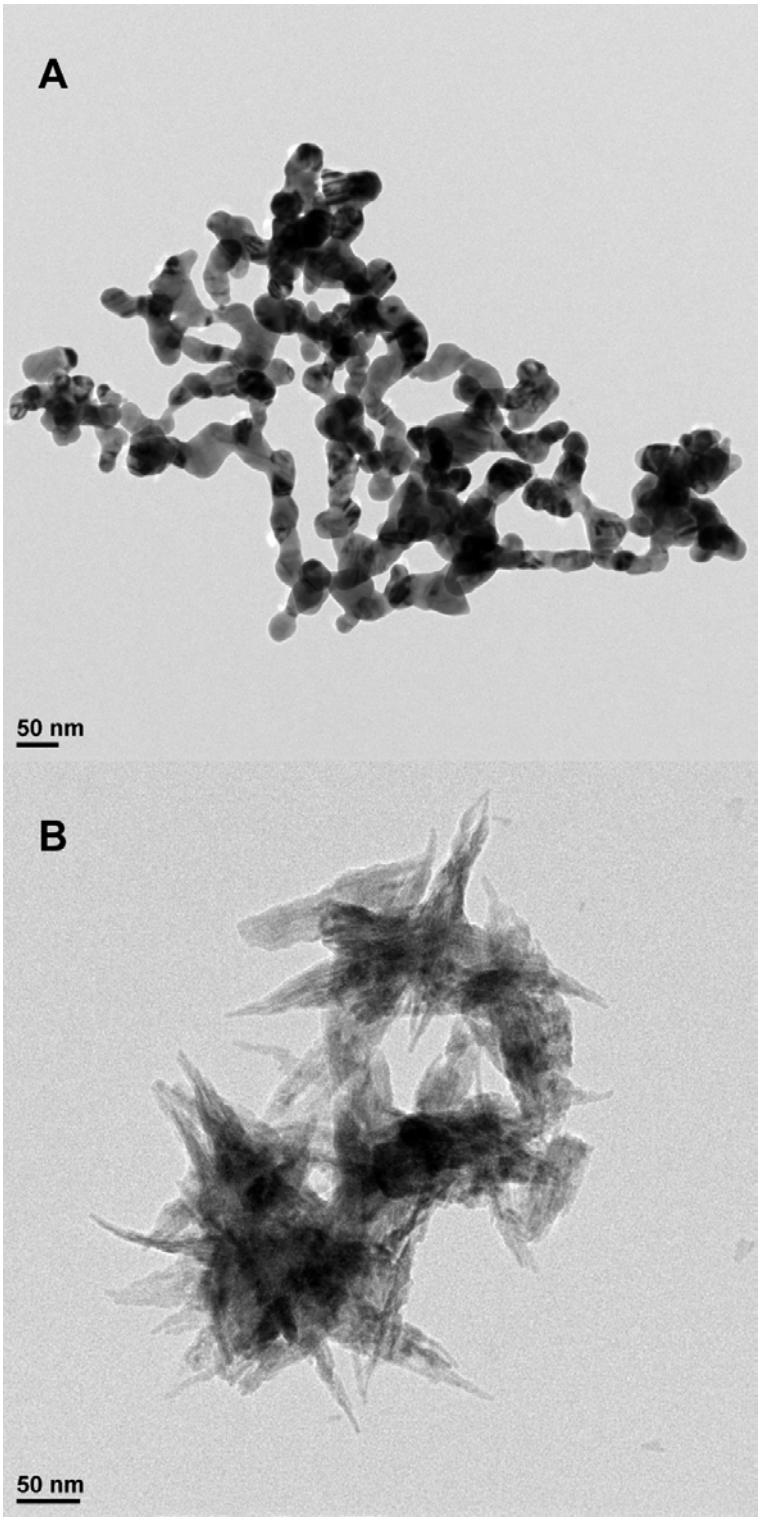

Figure 1. TEM images of the Ag (A) and Cu (B) nanostructures used in the spectroelectrochemical measurements.

Model and computational details. DFT was used to obtain calculated vibrational frequencies of the 4-ABT molecule, in gas phase and adsorbed on copper surfaces, as well as those of the 4,4'-DMAB. The model used for the metal surface consists in a flat metal cluster of 5 copper atoms arranged in two lines of 2 and 3 atoms with (111) orientation. The same cluster has been used by other groups to obtain calculated frequencies that agree well with experimental results. Previous studies with metal surfaces of low Miller indices have shown that experimental and harmonic calculated frequencies of adsorbed carboxylate anions do not depend significantly on the crystallographic orientation of the metal surface.[41-43] In the same way, we do not expect to have a significant effect of surface orientation on the vibrational bands of adsorbed 4-ABT and 4,4'-DMAB species. In addition, the small cluster size is not expected to significantly affect the calculated frequencies, as this is a local property. We do not report information regarding adsorption energies, as these are known to strongly depend on cluster size, especially for small clusters, as the one used in this work. The geometry of the metal cluster was kept fixed, with the copper nuclei located at their positions in the truncated crystal, and the same distances between neighbouring copper atoms as in the bulk metal (0.25562 nm).[44] The adsorbates are bonded to the metal cluster through their S atom, in a bridge configuration with the two atoms in the shorter metal row. A full optimization of the geometry of the free molecules and adsorbate system was carried out, using the functional of Perdew, Burke and Ernzehof as implemented in the Gaussian 03 code (PBEPBE).[45-47] This functional is known to give satisfactory results when dealing with adsorption systems. The copper atoms were described using the LANL2DZ effective core potential and associated double zeta basis set developed by Hay and Wadt.[48] A Pople type triple-zeta basis set with diffuse and polarization functions (6-311++G**)[49-50] was used for the C, N, S and H atoms. All frequency values were obtained for the optimized geometry, and are given

without scaling. Assignments of the calculated frequencies are based on the visualization of the vibrational normal modes using Molden.[51]

Spectroelectrochemical measurements. The SEIRA experiments were performed in a glass spectroelectrochemical cell [52] equipped with a prismatic silicon window beveled at 60° and using a gold wire and a AgCl/Ag electrode as the counter and the reference electrodes, respectively. A copper thin film chemically deposited on the silicon prism was used as the working electrode. These films were prepared by following the procedure described by Wang et al.[53] Briefly, this procedure includes a) the cleaning of the reflecting silicon surface with the RCA method,[54] b) the termination of the surface with hydrogen by immersion for 2 min in a 40% NH_4F (p.a. Merck) + 40% HF (Merck, suprapur) solution, c) the seeding of copper for 5-10 s in a 0.625 M HF + 3.15 mM $CuSO_4 \cdot 5\ H_2O$ (Merck, p.a.) solution and d) the electroless copper deposition for ca. 10 min in a plating solution containing 5 $g \cdot L^{-1}$ $CuSO_4 \cdot 5\ H_2O$, 25 $g \cdot L^{-1}$ $C_4H_4O_6KNa \cdot 4H_2O$ (potassium sodium tartrate, Probus, pure), 10 $mL \cdot L^{-1}$ HCHO (Merck, 37% p.a.) and 7 $g \cdot L^{-1}$ NaOH (Sigma Aldrich, reagent grade > 98% pellet anhydrous).[53] Under these conditions, a bright thin copper film was formed. After deposition, the sample was removed from the plating solution, thoroughly rinsed with plenty of ultrapure water, and dried in an argon stream. All the infrared spectra are presented in absorbance units (a.u.) and were obtained with a resolution of 8 cm^{-1} with a Nexus 8700 (Thermo Scientific) spectrometer equipped with a MCT-A detector. Sets of 100 interferograms were collected at increasing sample potentials in the 4-ABT-containing solution and plotted in absorbance units as $-\log(R/R_o)$, where R_o represents a reference single beam spectrum obtained from the same number of interferograms collected at –0.9 V before dosing 4-ABT.

SERS measurements were performed using the so-called nanoparticles-on-electrode approach.[10, 55-57] For SERS experiments, the nanostructured electrode was made by depositing a droplet of a metal nanostructure aqueous suspension with a pipette onto a polycrystalline polished Ag or Cu disk (3 mm in diameter each one) sheathed in a threaded poly(tetrafluoroethylene) (PTFE) piece. The droplet was dried in air for ~30 min. The substrate was then mounted on an electrochemical PTFE flow cell specifically designed for the in situ Raman measurements. A saturated AgCl/Ag electrode was used as reference electrode and a Pt wire was used as counter electrode. Raman spectra were obtained with a NRS-5000 Laser Raman Spectrometer (Jasco) and a Jovin-Ybon LabRam Specrometer. Four excitation lines were used: a 50 mW Nd-YAG laser at 532 nm, a 17 mW He–Ne laser at 632.8 nm, a 100 mW diode laser at 785 nm and a 500 mW Nd-YAG laser at 1064 nm. The visible laser beams were focused through a 50×longworking distance objective (0.5 NA) into a spot at the electrode surface. The NIR laser was focused through a 100x IR objective (0.85 NA). The size of the spot for the different lasers is primarily defined by the laser wavelength and microscope objective. Thus, the minimum achievable spot size is diffraction limited, according to the laws of physics and optics and can be calculated with the following expression:

$$\text{Minimum diameter} = 1.22\frac{\lambda}{NA}$$

where λ is the wavelength of the laser and NA is the numerical aperture of the microscope objective. Thus, the minimum diameters were 1.3, 1.5, 1.9 and 1.5 μm for the 532, 632.8, 785 and 1064 nm lasers. In addition, the power on the sample was 4, 2, 8 and 20 mW for the 532, 632.8, 785 and 1064 nm lasers. Thus, the power density can be directly calculated from the spot size and the power on the sample. For the 1064 nm laser, the focal distance of the 100x IR objective is so small that we could not work in the electrochemical cell, and dry experiments had

to be performed. For that purpose, after the deposition of the nanoparticles, a drop of the 10^{-3} M 4-ABT + 0.1 M $NaClO_4$ solution was deposited onto the nanoparticles and left over 20 minutes. After that time, the electrode was rinsed with 0.1 M $NaClO_4$ and then dried in an Ar atmosphere. The spectrometer resolution with the visible lasers was better than 5 cm^{-1} and the detectors employed were a Peltier-cooled charge coupled device (CCD) (1064×256 pixels) and an OMA-V InGaAs CCD (1024x1 pixels).

RESULTS

Cyclic voltammetry. Figure 2A and 2B show the voltammetric profiles for silver and copper massive electrodes in a 0.1 M $NaClO_4$ + 1 mM 4-ABT solution in the potential window of interest for the SERS and SEIRA experiments. In both cases, a reduction wave is observed, starting at about -0.8 V and -0.95 V for Ag and Cu, respectively. As recently reported, this process can be attributed to the electrochemical reductive desorption of the adsorbed 4-ABT molecules.[23] Additionally, oxidative currents are also observed starting at -0.30 and -0.40 V for Ag and Cu, respectively, attributed to the oxidation of 4-ABT.[23] Thus, the potential window between the oxidation and reduction of the adsorbed 4-ABT is rather similar for both metals (about 0.50-0.55 V). On the other hand, Figure 2C shows the curve corresponding to the 4,4'-DMAB reduction on a massive Cu electrode after previous adsorption in an ethanolic 4,4'-DMAB solution. The voltammogram shows clearly a reduction process starting at about -0.4 V that essentially disappears after a single reduction sweep, as expected from the adsorptive experimental conditions.

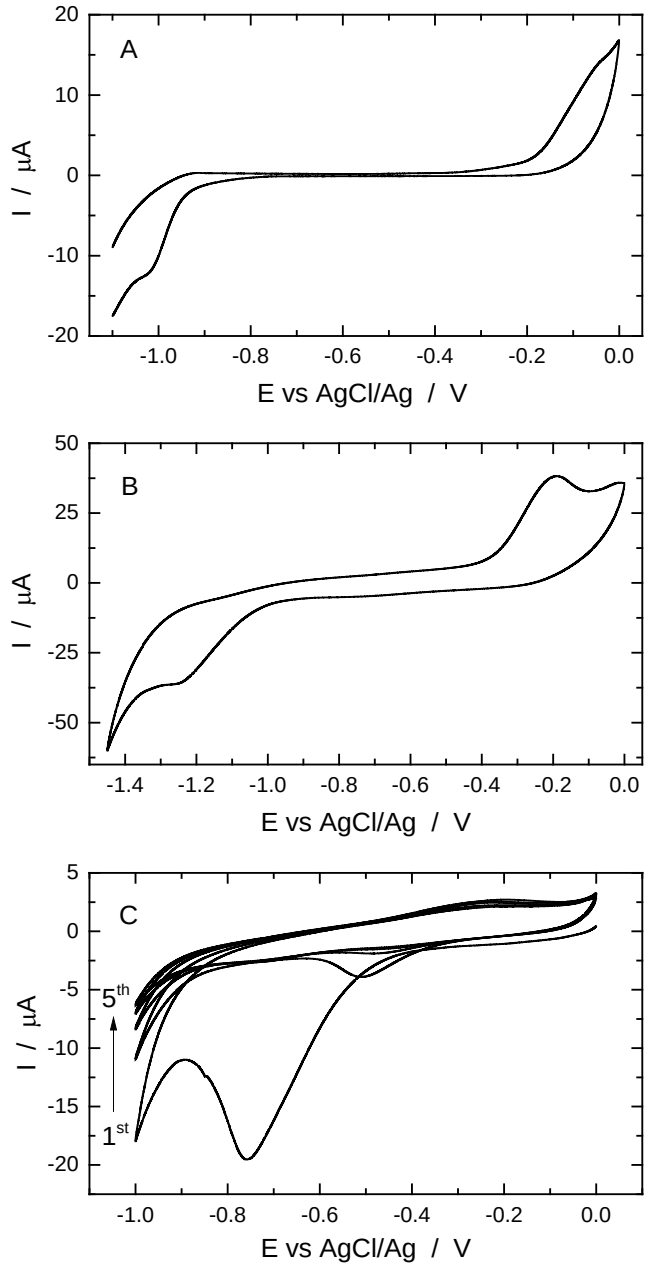

Figure 2. Cyclic voltammograms obtained with massive Ag (A) and Cu (B) electrodes in 0.1 M $NaClO_4$ + 10^{-3} M 4-ABT. Electrochemical response of a massive Cu electrode (C) in 0.1 M $NaClO_4$ after its immersion in a 10 times diluted ethanolic 4,4'-DMAB saturated solution. Scan rate: 50 mV s^{-1}.

Computational results. Table 1 summarizes the main unscaled calculated harmonic frequencies of 4-ABT both in gas phase and bonded to a small Cu cluster. These frequencies compare well with those in the experimental Raman spectrum for solid 4-ABT.

Table 1. Experimental (Raman and SERS) and calculated frequencies of 4-ABT (gas, PBE/6-311++G**; adsorbed on Cu, PBE/6-311++G**LANL2DZ).

Assignment[(a)]	Raman solid (exp.)[(b)]	SERS (exp.)[(b)]	4-ABT (gas) (calc.)	4-ABT (ad.) (calc.)
$\delta(NH_2) + \nu(CC)$ (a_1)	1618 w	-----	1614	1613
$\nu(CC)$ (a_1)	1595 vs	1591 s	1594	1594
	-----	1580 s [(c)]	-----	-----
$\nu(CC)$ (a_1)	1536 vw	-----	1564	1562
$\nu(CC) + \delta(CH)$ (a_1)	1490 w	1490 w	1480	1474
	-----	1434 vs [(c)]	-----	-----
$\nu(CC) + \delta(CH)$ (a_1)	1418 vw	1416 vw	1414	1414
	-----	1390 vs [(c)]	-----	-----
$\nu(CC) + \delta(CH)$ (a_1)	-----	-----	1343	1340
$\nu(CN) + \nu(CC)$ (a_1)	1310 w	1308 w	1282	1277
$\nu(CC) + \delta(CH)$ (a_1)	1272 w	1260 w	1276	1276
$\delta(CH)$ (a_1)	1172 s	1191 m	1163	1164
	-----	1144 vs [(c)]	-----	-----
$\nu(C\text{-}S) + \nu(CC)$ (a_1)	1090 vs	1080 m	1082	1071
$\delta(NH) + \delta(CH)$ (a_1)	1008 w	1008 w	1044	1047
$\delta(CCC)$ (a_1)	960 vw	950 vw	992	990

(a) All bendings in-plane unless otherwise stated.

(b) Experimental results of 4-ABT adsorbed on nanostructured Cu using a 632.8 nm laser and with a density power about 10^8 mW cm^{-2}.

(c) bands, the origin of which is not from 4-ABT.

The Figure 3A shows the simulated surface Raman spectrum of 4-ABT absorbed on Cu. The assignment of the experimental bands is based on the visualization of the vibrational normal modes obtained from the calculation of the adsorbed 4-ABT on the Cu cluster. An overall analysis of the theoretical frequencies shows that the bonding of the 4-ABT species to the metal cluster through the S atom has minimal influence on the frequencies. The most important difference is observed for the stretching of the C-S bond, which is shifted from 1082 to 1071 cm^{-1} upon adsorption on the cluster. Regarding the experimental frequencies for solid 4-ABT, and adsorbed on the Cu electrode, the effect of adsorption is also very small. The maximum differences amount to around 30 cm^{-1}, which corresponds to relative errors in wavenumbers of about or less than 3%.

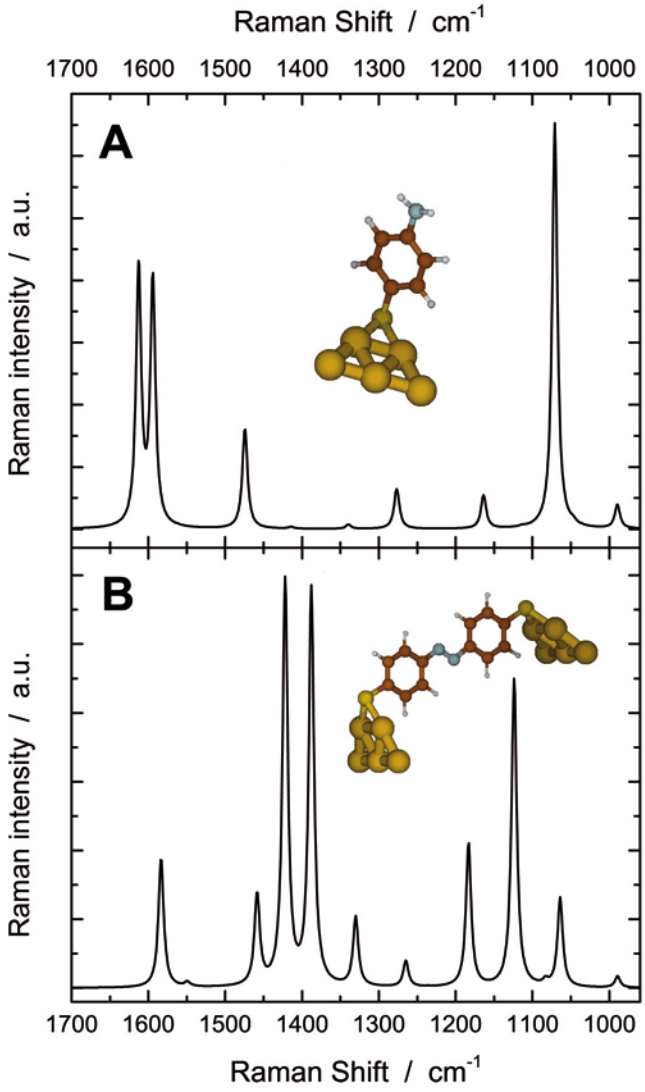

Figure 3. Calculated PBE/6-311++G** spectra and optimized geometries of 4-ABT (A) and 4-4'-DMAB (B) adsorbed on a Cu_5 metal cluster. The adsorbates are bonded to the metal through their S atom, in a bridge configuration with the two atoms in the shorter row.

A comparison of the frequencies of the experimental Raman bands with the theoretical harmonic frequencies obtained for 4-ABT adsorbed on Cu, indicates a good agreement. While some of the experimental and theoretical frequencies are almost coincident, the differences

between the experimental and calculated values can amount up to 40-50 cm^{-1}. Despite being these differences significantly higher than the experimental uncertainty ($8cm^{-1}$), the relative error is lower than 4% in the worst case. This quality compares well with the standards of other work in the field. Taking into account the simplicity of the model used for the calculation (small size of the cluster, no water present, absence of applied electric field, ...), and the errors inherent to the functional, the frequency results can be considered in overall as satisfactory, and sufficient to support the assignment of the normal mode to the experimental frequencies.

In the case of the 4,4'-DMAB species the comparison of experimental Raman frequencies with the theoretical harmonic frequencies for adsorbed species on Cu also shows a very good agreement for most modes. The Figure 3B shows the simulated surface Raman spectrum of 4,4'-DMAB absorbed on Cu. The most important numerical difference between Raman spectra corresponds to the C-C stretch in the mid 1300 cm^{-1} range, with a difference of about 45 cm^{-1}. The effect of adsorption on the calculated frequencies is very small, amounting to less than 10 cm^{-1} in most frequencies. In overall, we can conclude that the calculated and experimental values differ in less than 3%, which ensures a proper assignment of the experimental frequencies by comparison with the closest theoretical values. Finally, as it can be seen in Tables 1 and 2 the DFT calculations show that there are four bands that appear at 1135, 1388, 1422 and 1579 cm^{-1} for adsorbed 4,4'-DMAB that are absent for adsorbed 4-ABT. A similar lack is also observed when the experimental Raman spectra of both compounds are compared.

Table 2. Comparison of calculated frequencies of the 4,4'-DMAB in gas phase (PBE/6-311++G**), adsorbed on 2-Cu_5 clusters (PBE/6-311++G**,LANL2DZ) and experimental SERS and Raman frequencies.

Assignment	Raman* (exp.)	SERS** (exp.)	DMAB (gas) (calc.)	DMAB (ad.) (calc.)
ν (CC) + ν (NN) (a_g)	1588 vs	1591 m	1591	1584
ν (CC) (a_g)	-----	1579 m	1586	1579
ν (NN) + δ (CH) + ν (CC)	1481 m	1488 vw	1465	1459
δ (CH) + ν (CC) (a_g)	-----	-----	1463	1456
ν (NN) + δ (CH) + ν (CC)	1456 s	1434 vs	1427	1422
ν (NN) + ν (CC) (a_g)	1395 m	1390 vs	1393	1388
ν (CC) (a_g)	1306 w	1350 w	1338	1330
δ (CH) (a_g)	-----	-----	1273	1263
ν (CN) + δ (CH) + ν (CC)	1183 m	1180 m	1192	1183
ν (CN) + δ (CH) (a_g)	1147 vs	1144 vs	1138	1135
ν (C-S) + ν (CC) (a_g)	1064 m	1080 vs	1083	1086
δ (CCC) (a_g)	1002 w	1007 vw	991	990

(*) taken from reference [24]

(**) experimental results of 4,4'-DMAB adsorbed on the nanostructured Cu obtained with the laser at 632.8 nm and with a power density about 10^8 mW cm^{-2}.

SEIRAS. Taking into account the characteristics of the cyclic voltammetry of the 4-ABT on Cu reported in figure 2B, it is interesting to check whether the electrode potential alone could have some influence in the formation of new adsorbates on the Cu surface. One way to do this is

to analyze the potential-dependent behaviour of the infrared spectra of adsorbed 4-ABT. This kind of experiment is facilitated by the surface-enhanced absorption, which takes places when the probe molecule is adsorbed on a metal thin film (the so-called SEIRA effect [14, 58]). The method described by Wang et al. [53] provides an easy way to prepare thin copper films on silicon substrates showing high infrared absorption enhancements for adsorbed species. Potential-dependent infrared spectra of adsorbed 4-ABT on the chemically deposited copper film were obtained in SEIRAS experiments performed under attenuated total reflection (ATR) conditions (Kretschmann's configuration [14]). Figure 4 shows a set of ATR-SEIRA spectra collected at potentials ranging from -0.9 V (dosing potential) up to -0.10 V. These spectra are referred to the single beam spectrum collected at -0.9 V before dosing 4-ABT to the sodium perchlorate test solution. Thus, infrared bands related to adsorbed 4-ABT (as well as those for any other species not being present when collecting the reference spectrum) are expected to appear as positive-going features. The spectra obtained and shown in Figure 4 are similar to those previously reported by our group for 4-ABT adsorbed on a silver thin film electrode.[23]

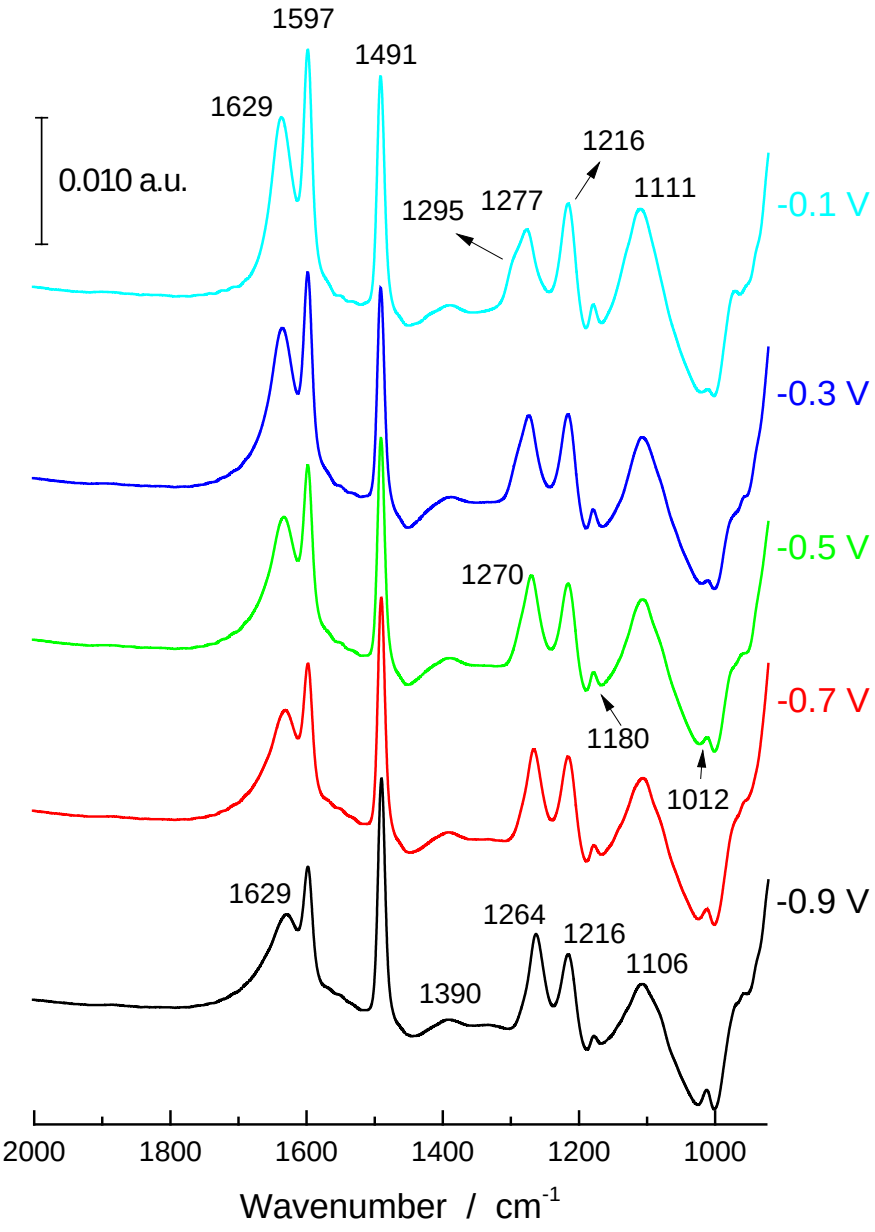

Figure 4. ATR-SEIRA spectra of 4-ABT on nanostructured Cu collected at potentials ranging from -0.9 V (dosing potential) up to -0.10 V.

Besides the bands at 1630 and 1106 cm^{-1}, which can be initially related to interfacial water and adsorbed perchlorate anions, respectively, the spectrum collected at -0.9 V shows bands at 1012, 1180, 1216, 1264, 1491, 1597 cm^{-1}. These latter bands will be also observed in the SERS spectrum (see below) of 4-ABT at this electrode potential. Main changes observed in the spectra collected at potentials above -0.90 V are related to an increase of the intensity of the bands at 1636 and 1106 cm^{-1} and the upward shift and broadening of the band initially at 1264 cm^{-1}. The development of the perchlorate band, which is observed with a similar potential-dependent behaviour in the SEIRA spectra collected for the copper thin film electrode in the 4-ABT-free sodium perchlorate solution, reflects the potential-dependent adsorption of co-adsorbed perchlorate anions, the surface coverage of which would increase as the electrode potential increases.

SERS. SERS spectra of a self-assembled monolayer of 4-ABT on copper surfaces decorated with copper nanostructures, using lasers at 532 nm, 632.8 nm and 785 nm as excitation sources, are shown in Figure 5. Different spectra are obtained depending on the electrode potential and the laser employed to record the SERS spectra. With the lasers at 532 nm (Figure 5A) and 632.8 nm (Figure 5B) a set of bands at 1008, 1080, 1144, 1191, 1390, 1434, 1580 and 1591 cm^{-1} are observed at potentials as low as -1.0 V but not when the laser used is at 785 nm (Figure 5C). With this laser, the complete set of bands is observed only at electrode potentials equal or higher than -0.6 V, while at lower potentials only bands at 1008, 1080, 1191, 1480 and 1596 cm^{-1} appear. These results for nanostructured Cu contrast with those observed when silver surfaces decorated with silver nanostructures are used as active SERS substrates. In addition, it is worthwhile mentioning the reversibility of the system. After reaching the higher potentials, by going back to -1 V (not shown) the initial spectrum is again recovered.

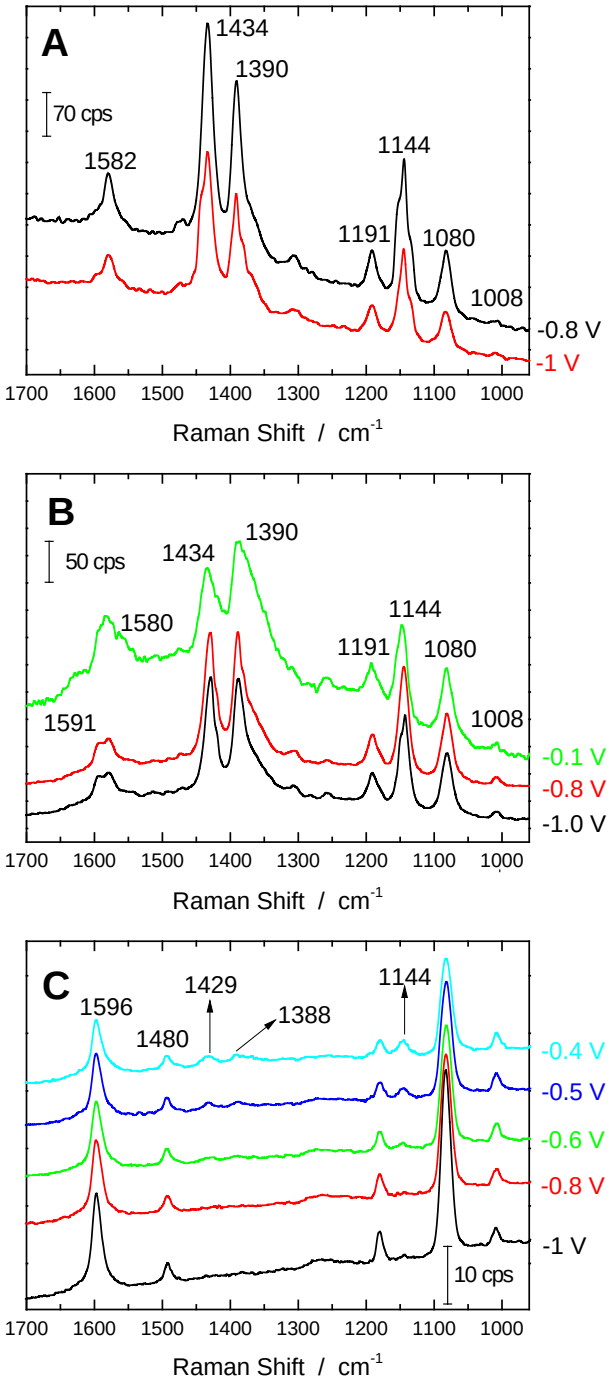

Figure 5. SERS spectra at different potentials of a self-assembled monolayer of 4-ABT from copper surfaces decorated with copper nanostructures, using lasers at 532 nm (acquisition time 10 s) (A), 632.8 nm (acquisition time 30 s) (B) and 785 nm (acquisition time 50 s) (C) as excitation sources. Laser power density about 10^8 mW cm^{-2}.

Figure 6 shows the SERS spectra obtained with silver at different potentials using the lasers at 532 nm and 785 nm. When the potential ranges from -0.9 V to -0.6 V only bands at 1008, 1080, 1191, 1480 and 1591 cm^{-1} can be observed. But for potentials higher than -0.6 V four new bands are visible at 1144, 1390, 1434 and 1575 cm^{-1} (as a shoulder). These results agree with previously observations by Tian et al.[24] who assigned these four bands to the 4,4'-DMAB molecules formed by photocatalytic oxidation of 4-ABT.

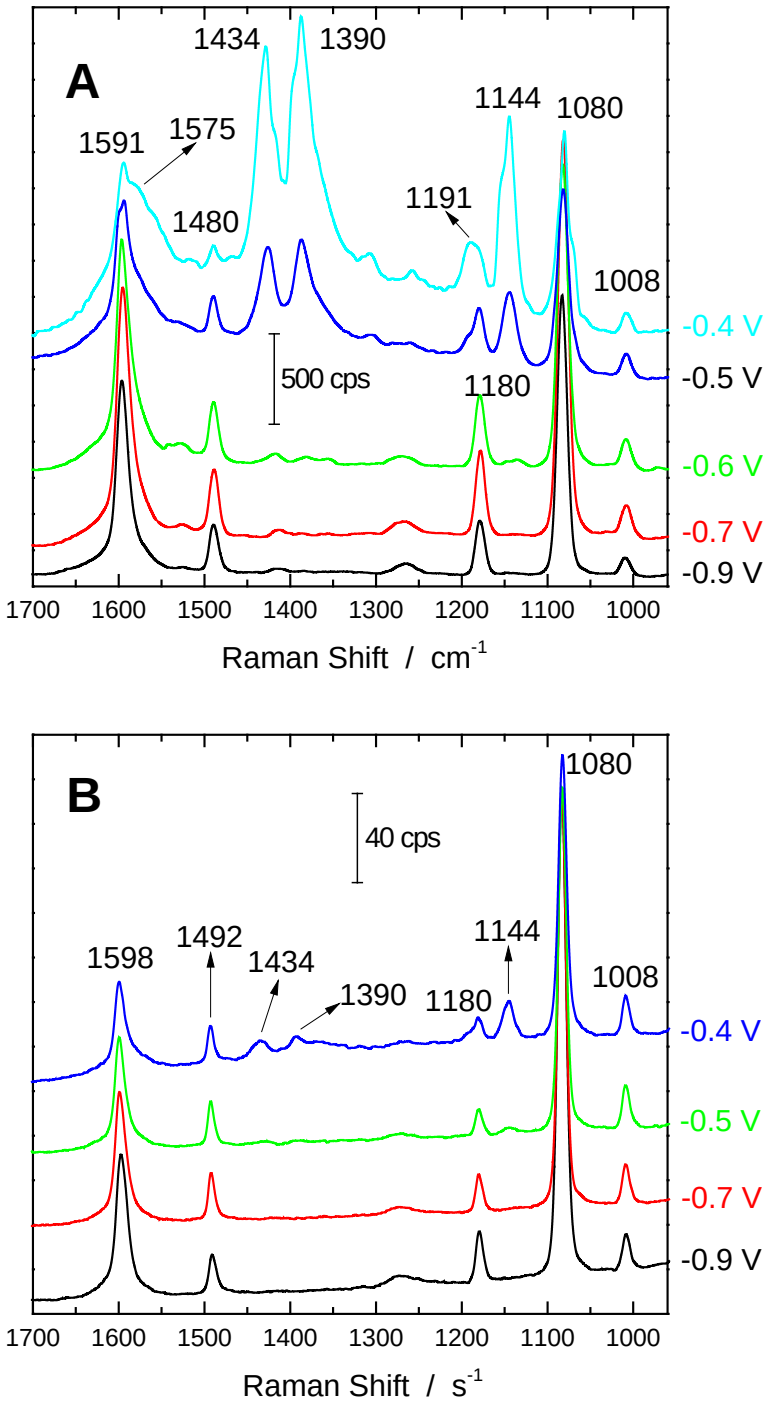

Figure 6. SERS spectra at different potentials of a self-assembled monolayer of 4-ABT from silver surfaces decorated with silver nanostructures using the lasers at 532 nm (acquisition time 5 s) (A) and 785 nm (acquisition time 25 s) (B). Laser power density about 10^8 mW cm^{-2}.

It is interesting to highlight that the ratio between the bands centred at 1434 cm^{-1} and 1390 cm^{-1} as well as that between the bands centred at 1390 cm^{-1} and 1144 cm^{-1} are similar both for Cu with the 632.8 nm laser and for Ag with the 532 nm regardless of the electrode potential, as those bands grow with the potential keeping the same ratio. On the other hand, the influence of the power density of the laser on the characteristics of the spectra of 4-ABT adsorbed on the nanostructured Cu is shown in Figure 7. Differences in the spectra can be observed when the power density of the 632.8 nm laser is decreased, by unfocusing it, from the initial value about 10^8 mW cm^{-2} (Figure 5B) to 10^3 mW cm^{-2} (Figure 7). At electrode potentials lower than -0.6 V the spectra are dominated by the bands at 1011, 1080, 1178 and 1595 cm^{-1} attributed to a_1 modes of the 4-ABT. However, for higher electrode potentials the spectra are similar to the obtained when the power density of the 632.8 nm laser is about 10^8 mW cm^{-2} (see Figure 5B).

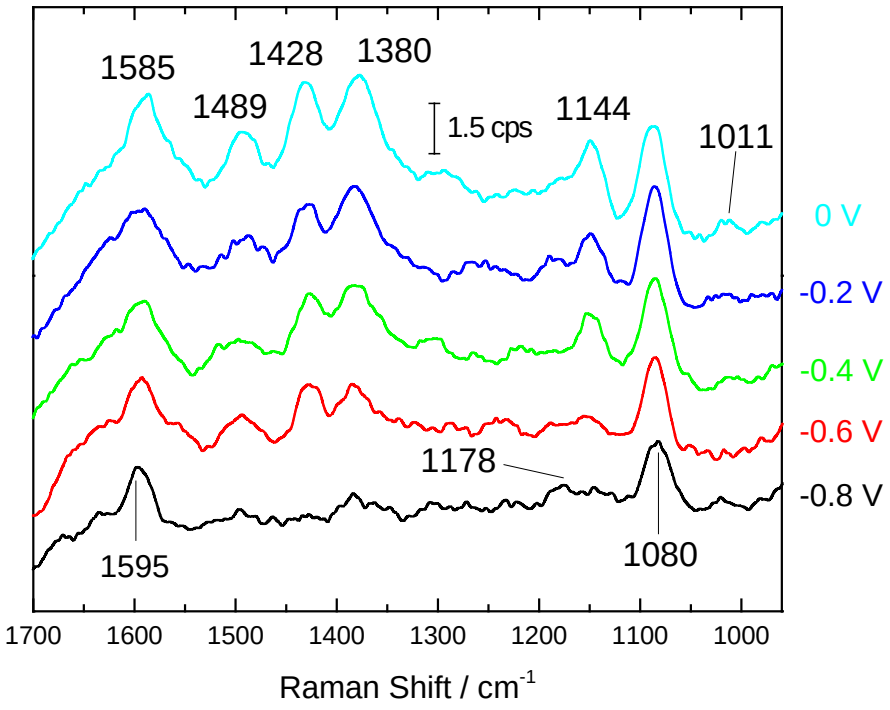

Figure 7. Potential dependent SERS of a self-assembled monolayer of 4-ABT from nanostructured copper surfaces spectra excited by a laser power density about 10^3 mW.cm^{-2} of the 632.8 nm laser. Acquisition time 90 s.

As it has been previously pointed out, 4,4'-DMAB was suggested to be formed from the adsorbed 4-ABT on Ag (and also on Au and Pt [23-24]) and to be responsible for the bands at 1144, 1390, 1434 and 1579 cm^{-1}. In order to check this, we have recorded the SERS spectra of the 4,4'-DMAB adsorbed on the nanostructured Cu obtained with the laser at 632.8 nm (Figure 8). The same set of bands observed for the 4-ABT (Figure 5B) at any electrode potential are recorded but with weak intensities for potentials lower than -0.6 V. For sake of comparison the spectrum obtained at low power density of the laser is also shown. In this case, only bands for the 4-ABT are observed. This behaviour will be explained later in connection with the voltammetric characteristics of the 4,4'-DMAB (Figure 2C). Finally, it is interesting to mention that we have not observed the presence of the band corresponding to the S-H bond of a trans-type 4,4'-DMAB linked to the metal only through a single S atom. Interestingly, this effect has been previously highlighted by Tian et al.[24] In addition, the missing signal of S-H was also observed in 1,4-benzenedithiol (BDT) by Kim's group.[59-60]

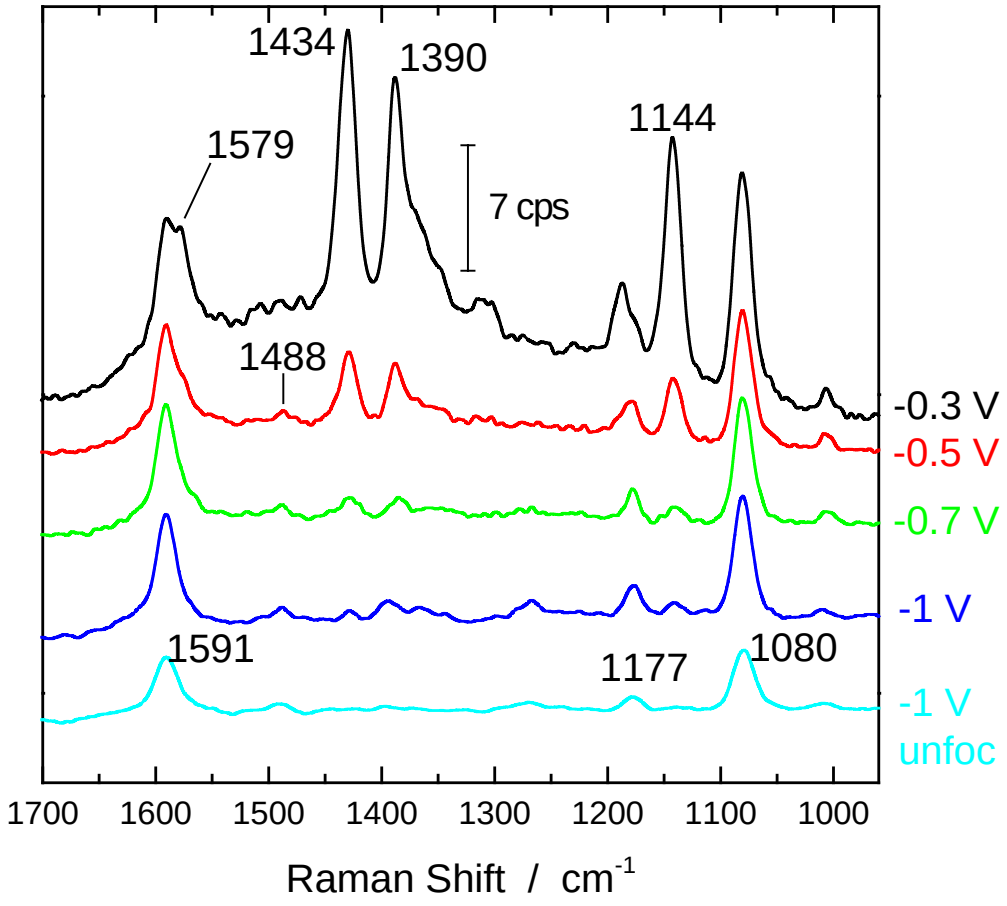

Figure 8. Potential dependent SERS spectra of the 4,4'-DMAB adsorbed on the nanostructured Cu obtained with the laser at 632.8 nm with a power density about 10^8 mW cm^{-2}. The spectrum at the bottom obtained with the same laser and a laser power density about 10^3 mW cm^{-2}. Acquisition time 30 s.

On the other hand, in order to deepen in the possible influence of the wavelength of the laser on the features of the spectra, the SERS spectra of a self-assembled monolayer of 4-ABT on nanostructured Cu and Ag surfaces are recorded and shown in Figure 9 using a 1064 nm laser and a laser power density about 10^9 mW cm^{-2}. Again, a set of bands similar to those observed

with the lasers at 532, 632.8 and 785 nm is obtained, which points out that the wavelength of the laser is not the crucial factor.

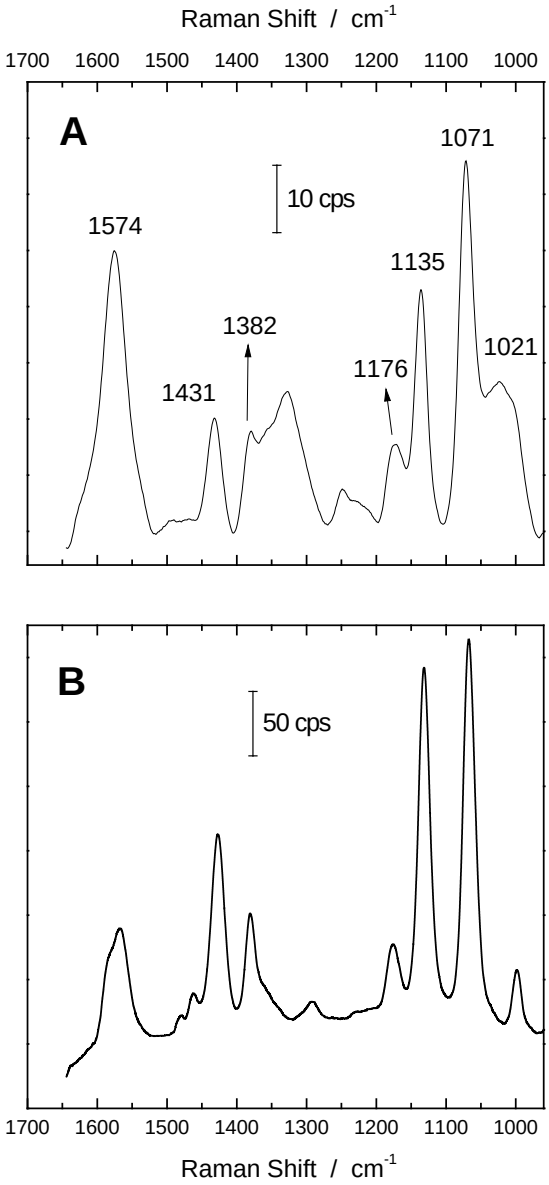

Figure 9. SERS spectra of 4-ABT adsorbed on nanostructured surfaces of Cu (A) and Ag (B) excited by a 1064 nm laser in absence of solution (without control of potential). Laser power density about 10^9 mW cm^{-2}. Acquisition time 30 s for Cu and 20 s for Ag.

Finally, we have recorded the SERS spectra for 4-ABT adsorbed on Cu (Figure 10A) and Ag (Figure 10B) at the same electrode potential (-0.4 V) in which no reduction process takes place (see Figures 2A and 2B). The spectra in these two figures were recorded both with the laser unfocused (spectra a) and focused (spectra b). In addition, and for sake of comparison, the SERS spectra of 4,4'-DMAB adsorbed on each one of the electrodes at the same potential and with the laser focused are also shown (spectra c).

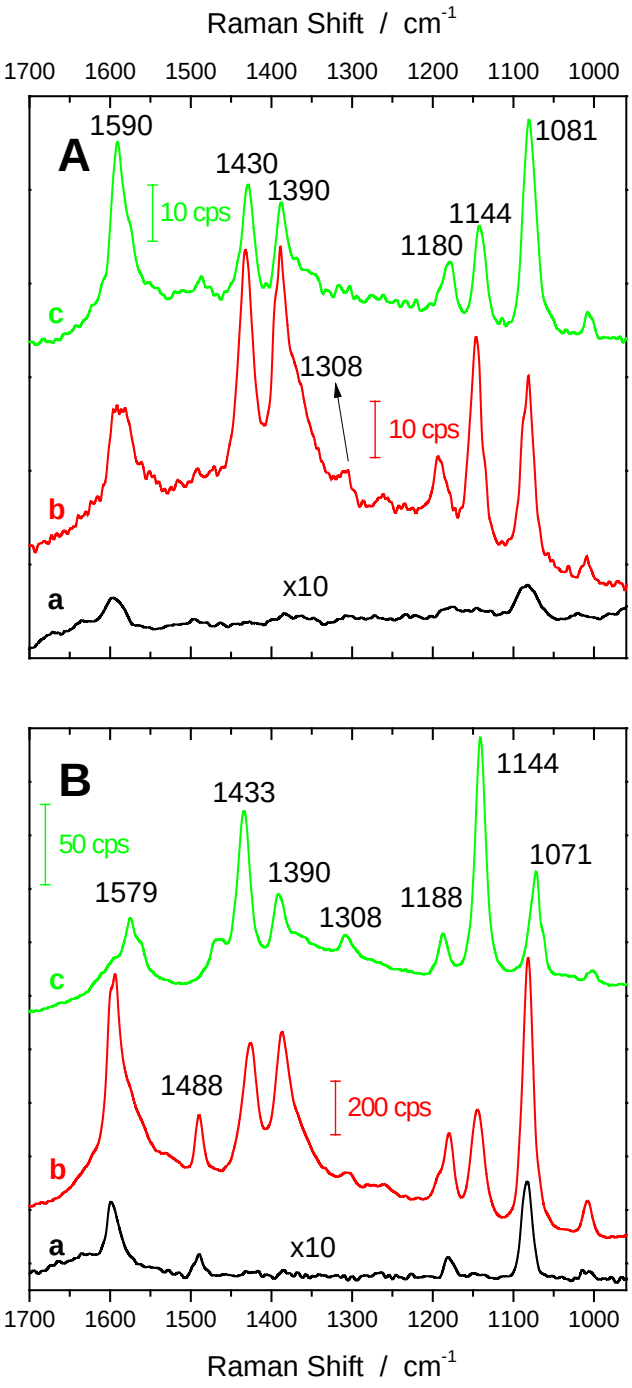

Figure 10. SERS spectra from 4-ABT (a and b) and 4,4'-DMAB (c) adsorbed on Cu (A) and Ag (B) at the same electrode potential (-0.4 V) for which no reduction process takes place with a 632.8 nm laser. Spectra (a) obtained with a laser power density about 10^3 mW cm^{-2} (acquisition time 60 s for Cu and 10 s for Ag). Spectra (b) (acquisition time 30 s for Cu and 5 s for Ag) and

(c) (acquisition time 30 s for Cu and Ag) obtained with a laser power density about 10^8 mW cm^{-2}.

DISCUSSION

The aim of this work is to study the behaviour of nanostructured Cu regarding the possible formation of 4,4'-DMAB from adsorbed 4-ABT and to compare the results obtained with those previously observed with Ag.[23] DFT calculations show that there are four bands that appear at 1135, 1388, 1422 and 1579 cm^{-1} for adsorbed 4,4'-DMAB on Cu which are absent for adsorbed 4-ABT likewise on Cu, and that a similar lack is also observed not only when the experimental Raman but also the SERS spectra are compared (see Tables 1 and 2).

According to the characteristics of the cyclic voltammetry of the 4-ABT on Cu reported in figure 2B, it is interesting to check whether only the effect of the electrode potential could have some influence in the formation of new adsorbates on the Cu surface. The main features of the SEIRA spectra for 4-ABT adsorbed on a copper thin film electrode, shown in Figure 4, are similar to those previously obtained for silver.[23] In this way, the spectrum collected at -0.9 V shows bands at 1012, 1106, 1180, 1216, 1264, 1390, 1491, 1597 and 1629 cm^{-1}. The bands at 1106, 1216 and 1629 cm^{-1} do not appear in the SERS spectrum of 4-ABT at this electrode potential (see Table 1). The band at 1106 cm^{-1}, related to the presence of co-adsorbed perchlorate anions (see below), hinders the observation of a small feature for adsorbed 4-ABT that was observed at 1084 cm^{-1} in the case of the silver electrode. A band at 1629 cm^{-1} could be tentatively assigned to the δ[NH] [32] of the amine group in the adsorbate. However, some contribution to this feature from the uncompensated (O-H) bending mode of interfacial water can be also expected in this spectral region. Finally, it is worth noting that the band appearing at

1216 cm^{-1} in Figure 4 does not seem to be related to adsorbed 4-ABT. This band is similar to that appearing at ca. 1225 cm^{-1} in the spectra reported by Wang et al.[53] for pyridine adsorbed on a copper electrode deposited on silicon. These authors suggested that this feature, which is absent when the copper electrode was deposited on germanium, was ascribed to the silicon substrate (namely to the O-Si-O stretching of silicon oxides formed on the exposed surface for metal-on-silicon electrodes). It has to be noted that, except for the features at 1225, 1106 and, probably, that at 1629 cm^{-1}, the bands in the spectrum obtained at -0.90 V in the 4-ABT-containing solution correspond to ring vibrations of the adsorbed 4-ABT molecules (see Table 1). An increase of the intensity of the bands at 1629 and 1106 cm^{-1} and the upward shift and broadening of the band initially at 1264 cm^{-1} are the main changes observed in the spectra collected at potentials above -0.90 V. The potential-dependent behaviour of the spectra in Figure 4 is rather similar to that reported for 4-ABT adsorbed on silver.[23] In this latter case, an additional small band was observed at ca. 1200 cm^{-1} which is obscured by the silicon feature at 1216 cm^{-1}. Thus, it can be concluded that both for Cu and Ag electrodes there are no extra bands in the infrared spectra associated to the oxidation of 4-ABT. The potential-dependent adsorption of co-adsorbed perchlorate anions, the surface coverage of which would increase as the electrode potential increases, is in the origin of the development of the perchlorate band which slightly shifts from 1106 cm^{-1} at -0.90 V to 1111 cm^{-1} at -0.10 V. It is also observed with a similar potential-dependent behaviour in the SEIRA spectra collected for the copper thin film electrode in the 4-ABT-free sodium perchlorate solution. The appearance of a net perchlorate absorption band in the spectrum collected at -0.90 V (Figure 4), not observed at this potential in the experiments carried out with silver electrodes can be interpreted as the result of an induced perchlorate adsorption process in the presence of adsorbed 4-ABT. In the same way, the increasing intensity

of the band at 1629 cm^{-1} in Figure 4 could be related to the coadsorption of interfacial water molecules associated to the perchlorate anions. In any case, it is clear from the spectra reported in Figure 4 that in absence of the laser excitation the 4,4'-DMAB is not produced from the adsorbed 4-ABT on nanostructured Cu in the whole range of potentials studied.

The next step in this study is to record potential-dependent SERS spectra of self-assembled monolayers of 4-ABT and 4,4'-DMAB on nanostructured Cu surfaces using lasers of different wavelengths and power densities. For sake of comparison the potential-dependent SERS spectra of self-assembled monolayers of 4-ABT on nanostructured Ag surfaces are also obtained with the same lasers and power densities. In agreement with previous findings,[24, 28, 32] the recorded SERS spectrum obtained with the laser at 532 nm changes significantly when the silver electrode potential is shifted from -0.9 V to -0.5 V (Figure 6A). Thus, four new bands are visible at 1144, 1390, 1434 and 1575 cm^{-1} (the latter one as a broad shoulder). As mentioned above, these bands were first considered to be a case of chemical enhancement [28] but later they have been assigned to different vibrational modes of 4,4'-DMBA [29] produced by a photocatalytic reaction of adsorbed 4-ABT. Surprisingly, when a copper massive electrode decorated with copper nanostructures is used, these bands are also observed with this laser at potentials as low as -1.0 V (Figure 5A). This behaviour also contrasts with that observed with Au and Pt.[23-24] It is known that Cu nanoparticles exhibit a plasmon absorption band with the maximum at wavelengths about of 580 nm (the exact values depending on their size, shape and aggregation).[61] Taken into account that aggregation shifts the plasmon resonance to higher values of wavelengths we have also recorded the SERS spectra of a self-assembled monolayer of 4-ABT on this active copper SERS substrate with a laser of 632.8 nm. Again, at potentials higher than -1.0 V, four bands

appear located at 1144, 1390, 1434 and 1580 cm^{-1} (Figure 5B). These bands cannot be assigned to the 4-ABT as shown in Table 1. Interestingly, Shin et al. [62] measured the SERS spectra of 4-nitrobenzenethiol on an activated Cu foil, under 632.8 nm radiation and without any potential control, and claimed the formation of 4-ABT, which was confirmed by the growing of calcium carbonate crystals selectively on the amine-terminated regions. However, if the SERS spectra are recorded with a lower power density (about 10^3 mW cm^{-2}) by simply unfocusing the laser, a dependence of the spectra with the potential is observed (Figure 7), similarly to that obtained with Ag [24] and Pt.[23] Under these conditions and at potentials equals or lower than -0.7 V the spectral feature is dominated by the bands at 1011, 1080, 1178 and 1595 cm^{-1} attributed to a_1 modes of 4-ABT (Table 1). This behaviour can be explained by taking into account the voltammetric response of 4,4'-DMAB on a Cu electrode in the potential region from -0.3 V to -1.0 V (first scan). As shown in Figure 2C, a clear cathodic contribution is observed from -0.5 V with a maximum current at about -0.75 V after which the hydrogen evolution reaction begins to be visible at potentials values below -0.9 V. In consequence, reduction of the 4,4'-DMAB molecules, eventually formed from 4-ABT, are thus expected. However, as shown in Figure 5B, this is not observed for Cu at high power density of the laser. This finding would suggest that in this case the reduction process does not compensate the photocatalytic process. To check this behaviour, we have studied the dependence with the potential of the SERS for 4,4'-DMAB on a Cu electrode in the potential region from -0.3 V to -1.0 V (Figure 8). The intensity of the four bands at 1144, 1390, 1434 and 1580 cm^{-1}, assigned to a_g modes of 4,4'-DMAB (see Table 2), decreases significantly as the electrode potential shifts to more negative values and becomes very weak at -1.0 V. In addition, at this potential if the power density of the laser is dropped at values about 10^3 $mWcm^{-2}$ the final spectrum is similar to the SERS spectrum of 4-ABT obtained in

analogous experimental conditions (Figure 7). This fact would support that the reduction of 4,4'-DMAB produces 4-ABT in this negative potential range. On the other hand, when the excitation wavelength is changed to 785 nm (Figure 5C) the electrode potential value at which the four bands located at 1144, 1388, 1429 and 1573 cm^{-1} (and assigned to 4,4'-DMBA formed from 4-ABT) appear is similar to that observed with Ag (Figure 6B). These results differ from those reported by Matejka et al.[36] where, in similar experimental conditions, that is, at the same wavelength and on a nanostructured Cu surface, these bands were not observed. They suggested that the higher affinity of Cu to nitrogen when compared to silver and gold would diminish at longer wavelengths (> 700 nm) the ability to form an azo-bond between two nitrogen atoms of neighbouring 4-ABT molecules. However, our spectra clearly confirm the formation of 4,4'-DMBA at this wavelength and at electrode potentials more positive than -0.5 V (Figure 5C). The potential-dependent behaviour of the SERS spectra observed when exciting with the diode laser at 785 nm could be explained taking into account that at this wavelength the excitation of the surface plasmon of Cu is not as efficient as at 632.8 nm.[61] Consequently, a poor yield in 4,4'-DMAB can be expected. In addition, and according with the voltammetric behaviour of 4,4'-DMAB on Cu (Figure 2C), a competitive reduction process exists in the range of potentials between -1.0 V and -0.5 V that would contribute to the consumption of the formed 4,4'-DMAB. The reduction process gives rise to the formation of 4-ABT as evidenced in the SERS spectra shown in Figure 8. For potentials more positive than -0.5 V the characteristic bands of 4,4'-DMAB can be clearly observed in Figures 5C and 6B. Finally, SERS spectra of a self-assembled monolayer of 4-ABT on Cu and Ag surfaces decorated with Cu and Ag nanostructures, respectively, were also recorded at 1064 nm excitation wavelength. The spectra obtained in absence of solution, that is, without control of the potential, are shown in Figures 9A and 9B.

Again, four bands at 1135, 1382, 1431 cm^{-1} and 1574 cm^{-1} are also observed as an evidence of the 4,4'-DMAB formation under the influence of the radiation at a wavelength as high as 1064 nm. Again, it is necessary to point out that these bands were not observed at this wavelength by Dendisova-Vyskovska et al.[35] using a colloidal Cu nanoparticle system. Taking into account the influence of the power density of the laser on the spectrum features, the absence of these bands could be probably related to the use of a FT-Raman spectrometer. In this regard, as it can be also seen in Figure 7 for a 632.8 nm laser, when the power density of the NIR laser is decreased (by unfocusing it for 4 μm) the quoted four bands attributed to 4,4'-DMAB disappear completely for Ag and almost for Cu. Thus, evidence of the formation of 4,4'-DMAB is observed even a wavelengths as high as 1064 nm.

In order to explain the results obtained with the different lasers we have to consider that a metal electrode can act either as an electron source (for reduction reactions) or as an electron sink (for oxidation reactions). The calculated energies of the HOMO and the LUMO of the adsorbed 4-ABT on Cu are -4.64 eV and -2.59 eV, respectively. The Fermi level value for bare Cu is -7.0 eV.[63] Taking into account the range of electrode potentials studies and that according with Trasatti [64] 0 V *versus* SHE corresponds to an electronic energy value of -4.44 eV, the Fermi level of the Cu electrodes is located between the HOMO and the LUMO of adsorbed 4-ABT. A similar explanation can be quoted for Ag.[65] In addition, the Fermi level can be tuned by varying the potential applied. If under appropriate conditions 4-ABT becomes oxidized, the electron transfer must occur from the adsorbate to the metal and two CT mechanisms can be claimed to act. The first mechanism is a photoinduced electron transfer that would occur from the 4-ABT HOMO to Cu if the photon of the laser had enough energy. Under these conditions, the excited

surface complex may follow two ways of deexcitation: a reverse CT back to the ground state followed by a radiative process or a photochemical reaction of the excited amino radical anion. The second CT mechanism is the creation of an electron-hole pair through surface plasmon activity. Each plasmon can decay into a photon (radiative process) or into a hot electron-hole pair (non-radiative process). The competition between these two processes depends on the characteristics of the plasmon, being the non-radiative process the dominant one for small nanoparticles or subradiant plasmon modes.[66] If a nearby electron donor is present, as the case of 4-ABT, a hot-hole could capture an electron from the HOMO and induce the formation of 4-ABT radicals followed by chemical coupling reactions. The hot electron will be quenched by oxygen or other oxidant. In this way it could greatly reduce the energy input requirements of the chemical transformation from 4-ABT to 4,4'-DMAB. Recently, Wu et al.[34] have investigated the electro-oxidation of 4-ABT on gold electrodes by means of DFT and they have proposed the formation of four different dimer products. Among them, the one formed by N-N coupling reaction of 4-ABT radicals would be the 4,4'-DMAB molecules the N=N stretchings of which are at the origin the bands about 1387 cm^{-1} and 1430 cm^{-1}. The excitation of surface plasmon in noble metal nanostructures by visible light is a very efficient process and shows excellent catalytic activity for water splitting [67-68] and Fenton's reaction.[69] Even excitation of surface plasmon resonance in metallic nanoparticles has been observed at wavelengths as high as 1064 nm.[70-71] On the other hand, Halas et al.[72] have shown that surface plasmon excited in the Au nanoparticle decays into hot electrons with energies that allow by energy transfer the dissociation of H_2 adsorbed on the Au nanoparticle surface. They have demonstrated that plasmon-excited nanoparticles can be an efficient source of hot electrons. Sun et al.[73] have investigated the substrate, wavelength and time dependence of the plasmon-assisted surface catalyzed

dimerization of 4-nitrobenzenethiol (4-NBT) to 4,4'-DMAB on Au, Ag and Cu films and they pointed out the participation in this case of hot electrons from plasmon decay in the dimerization process by previous reduction of 4-NBT by population of its LUMO orbital. Finally, as an evidence of the prevalence of the role of electron-hole pairs through surface plasmon activity we have recorded the SERS spectra for 4-ABT adsorbed on Cu (Figure 10A) and Ag (Figure 10B) at the same electrode potential (-0.4 V) in which no reduction process takes place, neither of 4-ABT nor of 4,4'-DMAB (see Figure 2). The spectra in these two figures were recorded with the laser unfocused (spectra a) and focused (spectra b). In addition, and for sake of comparison, the SERS spectra of 4,4'-DMAB adsorbed on each one of the electrodes at the same potential, and with the laser focused, are also shown (spectra c). As it can be seen in Figures 10A and 10B the characteristic bands of 4,4'-DMAB (spectra c) are present at -0.4 V in the spectra (b), but they are absent in the spectra (a). The only difference between spectra (a) and (b) is the corresponding power density of laser but not its photon energy. This conclusion agrees with the consideration of the surface oxidative reaction as a photoinduced catalyzed reaction.[53]

CONCLUSIONS

The theoretical and experimental results seem to support that the photoinduced surface catalytic formation of 4,4'-DMAB is produced by a surface oxidative reaction of 4-ABT adsorbed on nanostructured copper. From SEIRA spectra of 4-ABT adsorbed onto a copper film recorded at different electrode potentials it is concluded that no new species are formed only under electrochemical control. SERS spectra are consistent with the formation of the 4,4'-DMAB on both Cu and Ag nanostructured surfaces with the four used lasers (532 nm, 632.8 nm, 785 nm and 1064 nm). With the 532 nm and 632.8 nm lasers the 4,4'-DMAB would be formed

on Cu surface at electrode potentials as low as -1.0 V differently to the case of Ag (and others metals like Au and Pt), for which the electrode potential must reach values about -0.6 V. However, with the 785 nm laser the behaviour observed for Cu is similar to the other cited metals. Finally, the dependence of the SERS spectra of adsorbed 4-ABT and 4,4'-DMAB on nanostructured Cu with the power density of the laser at an electrode potential in which no reduction process takes place, seem to support the participation of a photoinduced catalyzed process.

AUTHOR INFORMATION

Corresponding Author

* Email: jmpm@ua.es

ACKNOWLEDGMENT

Financial support from Ministerio de Economía y Competitividad (projects CTQ2013-48280-C3-3-R and CTQ2013-44083-P), Fondos Feder, and the University of Alicante are greatly acknowledged. We are greatly thankful to Prof. Zhong_Qun Tian for providing the 4,4'-DMAB and to Dr. Roberto Gomez for useful discussions. We also thank William Cheuquepan for his help in the preparation of Cu thin films for SEIRA experiments and Dr. Jeronimo Juan from the SSTTI of the University of Alicante for experimental support.

REFERENCES

1. Fleischmann, M.; Hendra, P. J.; McQuillan, A. J. Raman Spectra of Pyridine Adsorbed at a Silver Electrode. *Chem. Phys. Lett.* **1974**, *26*, 163-166.
2. Moskovits, M. Surface-Enhanced Spectroscopy. *Reviews of Modern Physics* **1985**, *57*, 783-826.
3. Jeanmaire, D. L.; Van Duyne, R. P. Surface Raman Spectroelectrochemistry Part I. Heterocyclic, Aromatic, and Aliphatic Amines Adsorbed on the Anodized Silver Electrode. *J. Electroanal. Chem.* **1977**, *84*, 1-20.
4. Xu, H.; Bjerneld, E. J.; Käll, M.; Börjesson, L. Spectroscopy of Single Hemoglobin Molecules by Surface Enhanced Raman Scattering. *Phys. Rev. Lett.* **1999**, *83*, 4357-4360.
5. Lombardi, J. R.; Birke, R. L. A Unified View of Surface-Enhanced Raman Scattering. *Acc. Chem. Res.* **2009**, *42*, 734-742.
6. Otto, A. The 'Chemical' (Electronic) Contribution to Surface-Enhanced Raman Scattering. *J. Raman Spectrosc.* **2005**, *36*, 497-509.
7. Dong, B.; Liu, L.; Xu, H.; Sun, M. Experimental and Theoretical Evidence for the Chemical Mechanism in Serrs of Rhodamine 6g Adsorbed on Colloidal Silver Excited at 1064 Nm. *J. Raman Spectrosc.* **2010**, *41*, 719-720.
8. Akimov, A. V.; Mukherjee, A.; Yu, C. L.; Chang, D. E.; Zibrov, A. S.; Hemmer, P. R.; Park, H.; Lukin, M. D. Generation of Single Optical Plasmons in Metallic Nanowires Coupled to Quantum Dots. *Nature* **2007**, *450*, 402-406.
9. Fang, N.; Lee, H.; Sun, C.; Zhang, X. Sub Diffraction-Limited Optical Imaging with a Silver Superlens. *Science* **2005**, *308*, 534-537.
10. Gómez, R.; Pérez, J. M.; Solla-Gullón, J.; Montiel, V.; Aldaz, A. In Situ Surface Enhanced Raman Spectroscopy on Electrodes with Platinum and Palladium Nanoparticle Ensembles. *J. Phys. Chem. B* **2004**, *108*, 9943-9949.
11. Otto, A., Surface-Enhanced Raman Scattering: “Classical” and “Chemical” Origins. In *Light Scattering in Solids Iv*, Cardona, M.; Güntherodt, G., Eds. Springer Berlin Heidelberg: 1984; Vol. 54, pp 289-418.
12. Pettinger, B., In Situ Raman Spectroscopy at Metal Electrodes. In *Adsorption of Molecules at Metal Electrodes*, Lipkowski, J.; Ross, P. N., Eds. VCH Publishers: New York, 1992; pp 285-345.
13. Abdelsalam, M. E.; Mahajan, S.; Bartlett, P. N.; Baumberg, J. J.; Rusell, A. E. Sers at Structured Palladium and Platinum Surfaces. *J. Am. Chem. Soc.* **2007**, *129*, 7399-7406.
14. Osawa, M. Dynamic Processes in Electrochemical Reactions Studied by Surface-Enhanced Infrared Absorption Spectroscopy (Seiras). *Bull. Chem. Soc. Jpn.* **1997**, *70*, 2861-2880.
15. Osawa, M., In-Situ Surface-Enhanced Infrared Spectroscopy of the Electrode/Solution Interface. In *Adv. Electrochem. Sci. Eng.*, Wiley-VCH Verlag GmbH: 2008; pp 269-314.
16. Rodes, A.; Pérez, J. M.; Aldaz, A., Vibrational Spectroscopy. In *Handbook of Fuel Cells - Fundamentals, Technology and Applications*, Vielstich, W.; Lamm, A.; Gasteiger, H. A., Eds. John Wiley & Sons, Ltd: Chichester, 2003; Vol. 2.
17. Wandlowski, T.; Ataka, K.; Pronkin, S.; Diesing, D. Surface Enhanced Infrared Spectroscopy—Au(1 1 1-20 Nm)/Sulphuric Acid—New Aspects and Challenges. *Electrochim. Acta* **2004**, *49*, 1233-1247.

18. Aroca, R. F.; Ross, D. J.; Domingo, C. Surface-Enhanced Infrared Spectroscopy. *Appl. Spectrosc.* **2004**, *58*, 324A-338A.
19. Griffith, W. P.; Koh, T. Y. Vibrational Spectra of 1,2-Benzenedithiol, 2-Aminothiophenol and 2-Aminophenol and Their Ser Spectra. *Spectrochimica Acta Part A: Molecular and Biomolecular Spectroscopy* **1995**, *51*, 253-267.
20. Zhou, Q.; Zhao, G.; Chao, Y.; Li, Y.; Wu, Y.; Zheng, J. Charge-Transfer Induced Surface-Enhanced Raman Scattering in Silver Nanoparticle Assemblies. *J. Phys. Chem. C* **2007**, *111*, 1951-1954.
21. Zhou, Q.; Li, X.; Fan, Q.; Zhang, X.; Zheng, J. Charge Transfer Between Metal Nanoparticles Interconnected with a Functionalized Molecule Probed by Surface-Enhanced Raman Spectroscopy. *Angew. Chem. Int. Edit.* **2006**, *45*, 3970-3973.
22. Ward, D. R.; Halas, N. J.; Ciszek, J. W.; Tour, J. M.; Wu, Y.; Nordlander, P.; Natelson, D. Simultaneous Measurements of Electronic Conduction and Raman Response in Molecular Junctions. *Nano Lett.* **2008**, *8*, 919-924.
23. Vidal-Iglesias, F. J.; Solla-Gullón, J.; Rodes, A.; Feliu, J. M.; Pérez, J. M. Spectroelectrochemical Behavior of 4-Aminobenzenethiol on Nanostructured Platinum and Silver Electrodes. *Surf. Sci.* **2015**, *631*, 213-219.
24. Huang, Y. F.; Zhu, H. P.; Liu, G. K.; Wu, D. Y.; Ren, B.; Tian, Z. Q. When the Signal Is Not from the Original Molecule to Be Detected: Chemical Transformation of Para-Aminothiophenol on Ag During the Sers Measurement. *J. Am. Chem. Soc.* **2010**, *132*, 9244-9246.
25. Canpean, V.; Iosin, M.; Astilean, S. Disentangling Sers Signals from Two Molecular Species: A New Evidence for the Production of P,P′-Dimercaptoazobenzene by Catalytic Coupling Reaction of P-Aminothiophenol on Metallic Nanostructures. *Chem. Phys. Lett.* **2010**, *500*, 277-282.
26. Wu, D.-Y.; Zhao, L.-B.; Liu, X.-M.; Huang, R.; Huang, Y.-F.; Ren, B.; Tian, Z.-Q. Photon-Driven Charge Transfer and Photocatalysis of P-Aminothiophenol in Metal Nanogaps: A Dft Study of Sers. *Chem. Commun.* **2011**, *47*, 2520-2522.
27. Sun, M.; Huang, Y.; Xia, L.; Chen, X.; Xu, H. The Ph-Controlled Plasmon-Assisted Surface Photocatalysis Reaction of 4-Aminothiophenol to P,P′-Dimercaptoazobenzene on Au, Ag, and Cu Colloids. *J. Phys. Chem. c* **2011**, *115*, 9629-9636.
28. Osawa, M.; Matsuda, N.; Yoshii, K.; Uchida, I. Charge Transfer Resonance Raman Process in Surface-Enhanced Raman Scattering from P-Aminothiophenol Adsorbed on Silver: Herzberg-Teller Contribution. *J. Phys. Chem.* **1994**, *98*, 12702-12707.
29. Richter, A. P.; Lombardi, J. R.; Zhao, B. Size and Wavelength Dependence of the Charge-Transfer Contributions to Surface-Enhanced Raman Spectroscopy in Ag/Patp/Zno Junctions. *J. Phys. Chem. c* **2010**, *114*, 1610-1614.
30. Kim, K.; Yoon, J. K.; Lee, H. B.; Shin, D.; Shin, K. S. Surface-Enhanced Raman Scattering of 4-Aminobenzenethiol in Ag Sol: Relative Intensity of A1- and B2-Type Bands Invariant Against Aggregation of Ag Nanoparticles. *Langmuir* **2011**, *27*, 4526-4531.
31. Kim, K.; Lee, H. B.; Shin, D.; Ryoo, H.; Lee, J. W.; Shin, K. S. Surface-Enhanced Raman Scattering of 4-Aminobenzenethiol on Silver: Confirmation of the Origin of B2-Type Bands. *J. Raman Spectrosc.* **2011**, *42*, 2112-2118.
32. Huang, Y. F.; Wu, D. Y.; Zhu, H. P.; Zhao, L. B.; Liu, G. K.; Ren, B.; Tian, Z. Q. Surface-Enhanced Raman Spectroscopic Study of P-Aminothiophenol. *Phys. Chem. Chem. Phys.* **2012**, *14*, 8485-8497.

33. Cao, L.; Diao, P.; Tong, L.; Zhu, T.; Liu, Z. Surface-Enhanced Raman Scattering of P-Aminothiophenol on a Au(Core)/Cu(Shell) Nanoparticle Assembly. *ChemPhysChem* **2005**, *6*, 913-918.
34. Zhao, L.-B.; Zhang, M.; Ren, B.; Tian, Z.-Q.; Wu, D.-Y. Theoretical Study on Thermodynamic and Spectroscopic Properties of Electro-Oxidation of P-Aminothiophenol on Gold Electrode Surfaces. *J. Phys. Chem. C* **2014**, *118*, 27113-27122.
35. Dendisová-Vyškovská, M.; Prokopec, V.; Člupek, M.; Matějka, P. Comparison of Sers Effectiveness of Copper Substrates Prepared by Different Methods: What Are the Values of Enhancement Factors? *J. Raman Spectrosc.* **2012**, *43*, 181-186.
36. Dendisová, M.; Havránek, L.; Ončák, M.; Matějka, P. In Situ Sers Study of Azobenzene Derivative Formation from 4-Aminobenzenethiol on Gold, Silver, and Copper Nanostructured Surfaces: What Is the Role of Applied Potential and Used Metal? *J. Phys. Chem. C* **2013**, *117*, 21245-21253.
37. López-Cudero, A.; Solla-Gullón, J.; Herrero, E.; Aldaz, A.; Feliu, J. M. Co Electrooxidation on Carbon Supported Platinum Nanoparticles: Effect of Aggregation. *J. Electroanal. Chem.* **2010**, *644*, 117-126.
38. Sanchez-Sanchez, C. M.; Vidal-Iglesias, F. J.; Solla-Gullon, J.; Montiel, V.; Aldaz, A.; Feliu, J. M.; Herrero, E. Scanning Electrochemical Microscopy for Studying Electrocatalysis on Shape-Controlled Gold Nanoparticles and Nanorods. *Electrochim. Acta* **2010**, *55*, 8252-8257.
39. Erikson, H.; Sarapuu, A.; Tammeveski, K.; Solla-Gullon, J.; Feliu, J. M. Shape-Dependent Electrocatalysis: Oxygen Reduction on Carbon-Supported Gold Nanoparticles. *ChemElectroChem* **2014**, *1*, 1338-1347.
40. Lugaresi, O.; Perales-Rondón, J. V.; Minguzzi, A.; Solla-Gullón, J.; Rondinini, S.; Feliu, J. M.; Sánchez-Sánchez, C. M. Rapid Screening of Silver Nanoparticles for the Catalytic Degradation of Chlorinated Pollutants in Water. *Applied Catalysis B: Environmental* **2015**, *163*, 554-563.
41. Delgado, J. M.; Rodes, A.; Orts, J. M. B3lyp and in Situ Atr-Seiras Study of the Infrared Behavior and Bonding Mode of Adsorbed Acetate Anions on Silver Thin-Film Electrodes. *J. Phys. Chem. C* **2007**, *111*, 14476-14483.
42. Berna, A.; Delgado, J. M.; Orts, J. M.; Rodes, A.; Feliu, J. M. Spectroelectrochemical Study of the Adsorption of Acetate Anions at Gold Single Crystal and Thin-Film Electrodes. *Electrochim. Acta* **2008**, *53*, 2309-2321.
43. Delgado, J. M.; Blanco, R.; Orts, J. M.; Pérez, J. M.; Rodes, A. Dft and in-Situ Spectroelectrochemical Study of the Adsorption of Fluoroacetate Anions at Gold Electrodes. *J. Phys. Chem. C* **2009**, *113*, 989-1000.
44. Lide, D. R., *Crc Handbook of Chemistry and Physics: A Ready-Reference Book of Chemical and Physical Data*; CRC Press, 2005.
45. Perdew, J. P.; Burke, K.; Ernzerhof, M. Generalized Gradient Approximation Made Simple. *Phys. Rev. Lett.* **1996**, *77*, 3865-3868.
46. Perdew, J. P.; Burke, K.; Ernzerhof, M. Generalized Gradient Approximation Made Simple [Phys. Rev. Lett. 77, 3865 (1996)]. *Phys. Rev. Lett.* **1997**, *78*, 1396-1396.
47. Frisch, M. J.; Trucks, G. W.; Schlegel, H. B.; Scuseria, G. E.; Robb, M. A.; Cheeseman, J. R.; Montgomery, J. A.; Vreven, T.; Kudin, K. N.; Burant, J. C. et al. Gaussian 03, Revision D.02. Gaussian 03, Rev. D.02, Wallingdorf CT, 2004.
48. Hay, P. J.; Wadt, W. R. Ab Initio Effective Core Potentials for Molecular Calculations. Potentials for K to Au Including the Outermost Core Orbitale. *J. Chem. Phys.* **1985**, *82*, 299-310.

49. McLean, A. D.; Chandler, G. S. Contracted Gaussian Basis Sets for Molecular Calculations. I. Second Row Atoms, Z=11–18. *J. Chem. Phys.* **1980**, *72*, 5639-5648.
50. Krishnan, R.; Binkley, J. S.; Seeger, R.; Pople, J. A. Self-Consistent Molecular Orbital Methods. Xx. A Basis Set for Correlated Wave Functions. *J. Chem. Phys.* **1980**, *72*, 650-654.
51. Schaftenaar, G.; Noordik, J. H. Molden: A Pre- and Post-Processing Program for Molecular and Electronic Structures. *J. Comput.-Aided Mol. Des.* **2000**, *14*, 123-134.
52. Delgado, J. M.; Orts, J. M.; Rodes, A. Atr-Seiras Study of the Adsorption of Acetate Anions at Chemically Deposited Silver Thin Film Electrodes. *Langmuir* **2005**, *21*, 8809-8816.
53. Wang, H.-F.; Yan, Y.-G.; Huo, S.-J.; Cai, W.-B.; Xu, Q.-J.; Osawa, M. Seeded Growth Fabrication of Cu-on-Si Electrodes for in Situ Atr-Seiras Applications. *Electrochim. Acta* **2007**, *52*, 5950-5957.
54. Kern, W.; Puotinen, D. A., Cleaning Solutions Based on Hydrogen for Use in Silicon Semiconductor Technology. *R.C.A. Review* **1970**, *31*, 187-206.
55. Gómez, R.; Solla-Gullón, J.; Pérez, J. M.; Aldaz, A. Surface-Enhanced Raman Spectroscopy Study of Ethylene Adsorbed on a Pt Electrode Decorated with Pt Nanoparticles. *ChemPhysChem* **2005**, *6*, 2017-2021.
56. Gómez, R.; Solla-Gullón, J.; Pérez, J. M.; Aldaz, A. Nanoparticles-on-Electrode Approach for in Situ Surface-Enhanced Raman Spectroscopy Studies with Platinum-Group Metals: Examples and Prospects. *J. Raman Spectrosc.* **2005**, *36*, 613-622.
57. Vidal-Iglesias, F. J.; Solla-Gullon, J.; Perez, J. M.; Aldaz, A. Evidence by Sers of Azide Anion Participation in Ammonia Electrooxidation in Alkaline Medium on Nanostructured Pt Electrodes. *Electrochem. Commun.* **2006**, *8*, 102-106.
58. Aroca, R., *Surface Enhanced Vibrational Spectroscopy*; John Wiley & Sons Ltd: Chichester (UK), 2006.
59. Cho, S. H.; Han, H. S.; Jang, D.-J.; Kim, K.; Kim, M. S. Raman Spectroscopic Study of 1,4-Benzenedithiol Adsorbed on Silver. *J. Phys. Chem.* **1995**, *99*, 10594-10599.
60. Joo, S. W.; Han, S. W.; Kim, K. Adsorption of 1,4-Benzenedithiol on Gold and Silver Surfaces: Surface-Enhanced Raman Scattering Study. *J. Colloid Interface Sci.* **2001**, *240*, 391-399.
61. Johnson, R. C.; Li, J.; Hupp, J. T.; Schatz, G. C. Hyper-Rayleigh Scattering Studies of Silver, Copper, and Platinum Nanoparticle Suspensions. *Chem. Phys. Lett.* **2002**, *356*, 534-540.
62. Shin, K. S.; Lee, H. S.; Joo, S. W.; Kim, K. Surface-Induced Photoreduction of 4-Nitrobenzenethiol on Cu Revealed by Surface-Enhanced Raman Scattering Spectroscopy. *J. Phys. Chem. C* **2007**, *111*, 15223-15227.
63. Ashcroft, N. W.; Mermin, N. D., *Solid State Physics*; Holt, Rinehart and Winston, 1976.
64. Trasatti, S. Absolute Electrode Potential: An Explanatory Note. *Pure Appl. Chem.* **1986**, *58*, 955-966.
65. Zhao, L.-B.; Huang, Y.-F.; Liu, X.-M.; Anema, J. R.; Wu, D.-Y.; Ren, B.; Tian, Z.-Q. A Dft Study on Photoinduced Surface Catalytic Coupling Reactions on Nanostructured Silver: Selective Formation of Azobenzene Derivatives from Para-Substituted Nitrobenzene and Aniline. *Phys. Chem. Chem. Phys.* **2012**, *14*, 12919-12929.
66. Willingham, B.; Link, S. Energy Transport in Metal Nanoparticle Chains Via Sub-Radiant Plasmon Modes. *Opt. Express* **2011**, *19*, 6450-6461.
67. Gomes Silva, C.; Juárez, R.; Marino, T.; Molinari, R.; García, H. Influence of Excitation Wavelength (Uv or Visible Light) on the Photocatalytic Activity of Titania Containing Gold

Nanoparticles for the Generation of Hydrogen or Oxygen from Water. *J. Am. Chem. Soc.* **2010**, *133*, 595-602.
68. Ingram, D. B.; Linic, S. Water Splitting on Composite Plasmonic-Metal/Semiconductor Photoelectrodes: Evidence for Selective Plasmon-Induced Formation of Charge Carriers Near the Semiconductor Surface. *J. Am. Chem. Soc.* **2011**, *133*, 5202-5205.
69. Navalon, S.; de Miguel, M.; Martin, R.; Alvaro, M.; Garcia, H. Enhancement of the Catalytic Activity of Supported Gold Nanoparticles for the Fenton Reaction by Light. *J. Am. Chem. Soc.* **2011**, *133*, 2218-2226.
70. Nishijima, Y.; Ueno, K.; Yokota, Y.; Murakoshi, K.; Misawa, H. Plasmon-Assisted Photocurrent Generation from Visible to Near-Infrared Wavelength Using a Au-Nanorods/Tio2 Electrode. *J. Phys. Chem. Lett.* **2010**, *1*, 2031-2036.
71. Mao, Z.; Song, W.; Chen, L.; Ji, W.; Xue, X.; Ruan, W.; Li, Z.; Mao, H.; Ma, S.; Lombardi, J. R. et al. Metal–Semiconductor Contacts Induce the Charge-Transfer Mechanism of Surface-Enhanced Raman Scattering. *J. Phys. Chem. C* **2011**, *115*, 18378-18383.
72. Mukherjee, S.; Libisch, F.; Large, N.; Neumann, O.; Brown, L. V.; Cheng, J.; Lassiter, J. B.; Carter, E. A.; Nordlander, P.; Halas, N. J. Hot Electrons Do the Impossible: Plasmon-Induced Dissociation of H2 on Au. *Nano Lett.* **2013**, *13*, 240-247.
73. Dong, B.; Fang, Y.; Chen, X.; Xu, H.; Sun, M. Substrate-, Wavelength-, and Time-Dependent Plasmon-Assisted Surface Catalysis Reaction of 4-Nitrobenzenethiol Dimerizing to P,P′-Dimercaptoazobenzene on Au, Ag, and Cu Films. *Langmuir* **2011**, *27*, 10677-10682.

Table of Contents Graphic

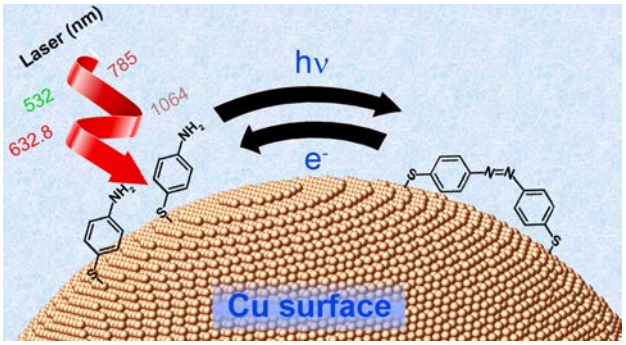

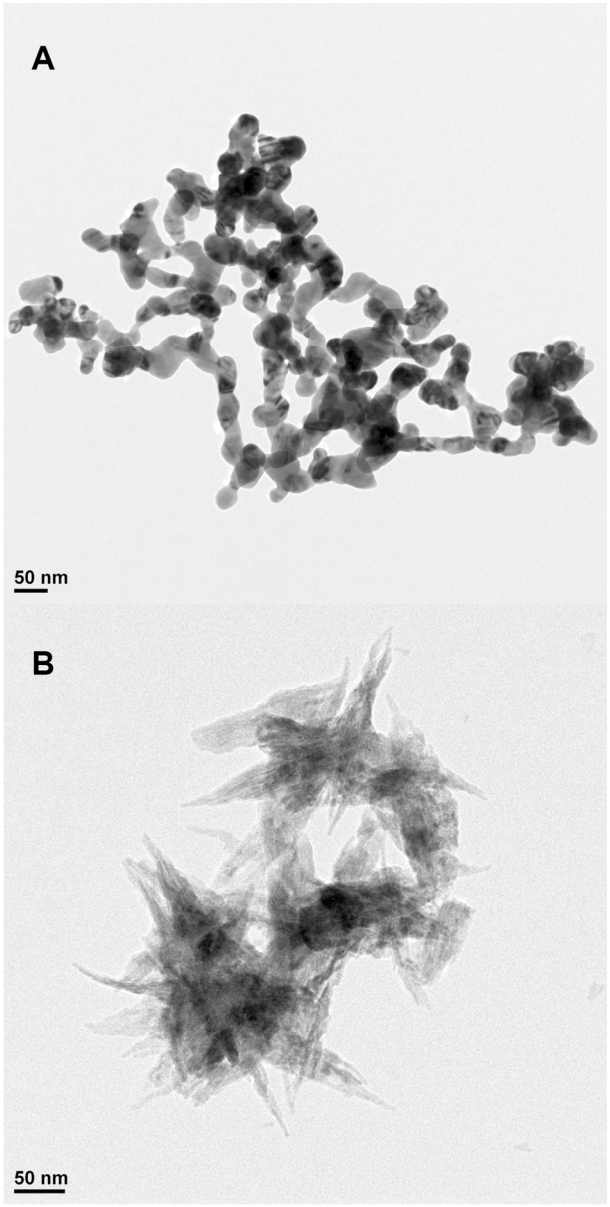

Figure 1. TEM images of the Ag (A) and Cu (B) nanostructures used in the spectroelectrochemical measurements.
85x168mm (300 x 300 DPI)

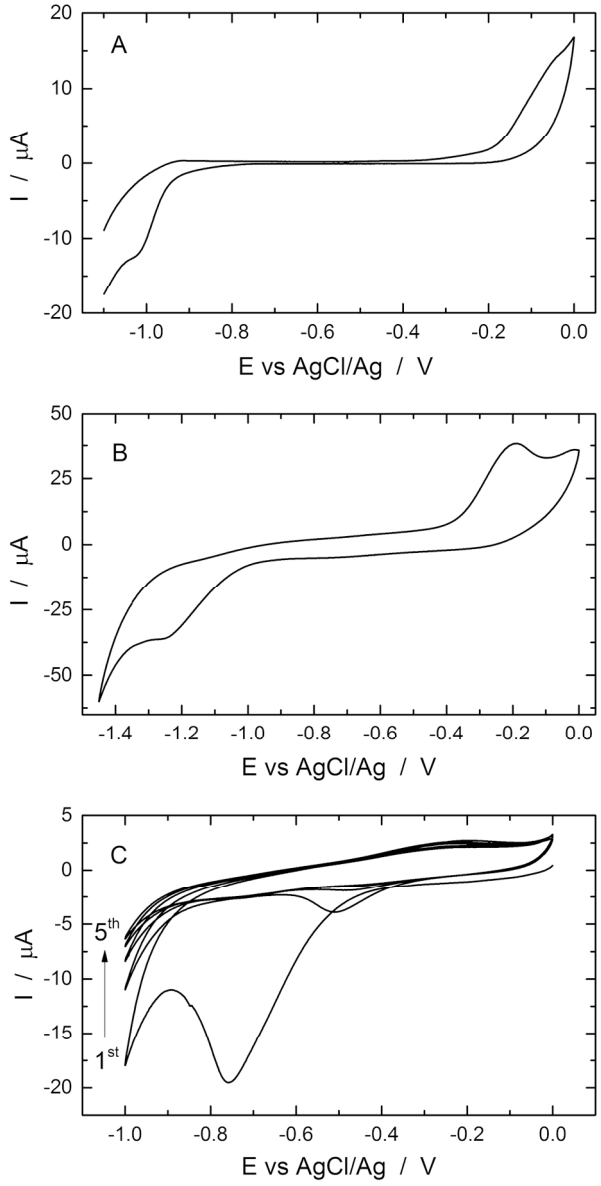

Figure 2. Cyclic voltammograms obtained with massive Ag (A) and Cu (B) electrodes in 0.1 M NaClO4 + 10-3 M 4-ABT. Electrochemical response of a massive Cu (C) in 0.1 M NaClO4 after its immersion in a 10 times diluted ethanolic 4,4'-DMAB saturated solution. Scan rate: 50 mV s-1.
108x203mm (300 x 300 DPI)

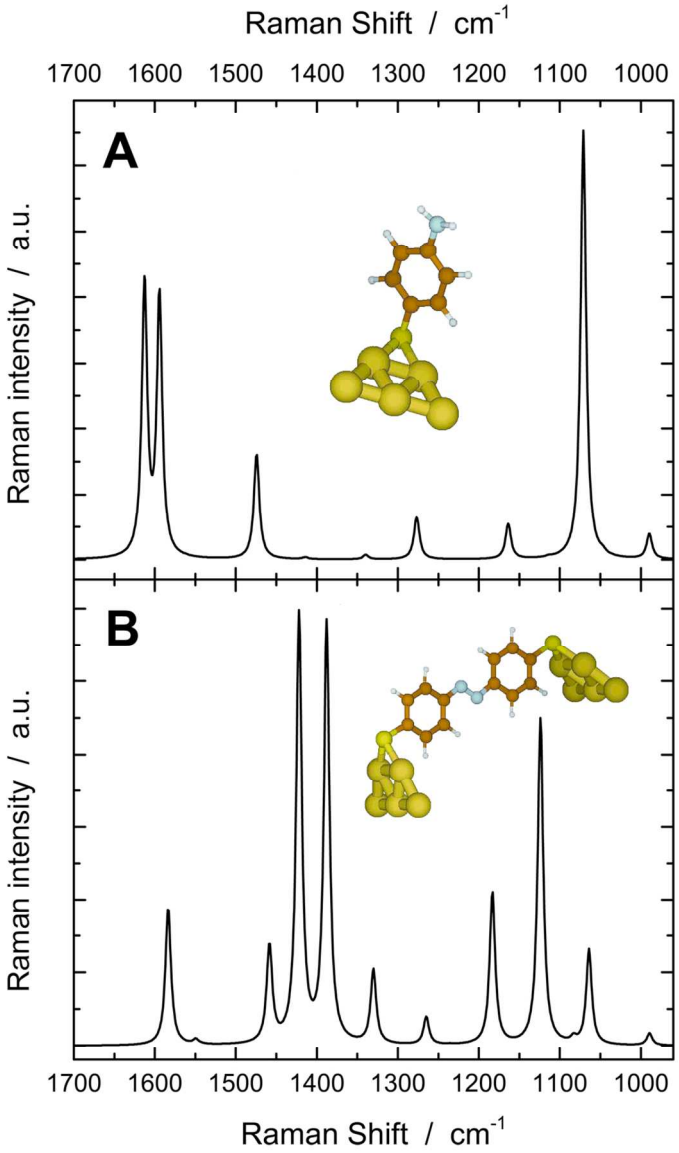

Figure 3. Calculated PBE/6-311++G** spectra and optimized geometries of 4-ABT (A) and 4-4'-DMAB (B) adsorbed on a Cu5 metal cluster. The adsorbates are bonded to the metal through their S atom, in a bridge configuration with the two atoms in the shorter row.
99x150mm (300 x 300 DPI)

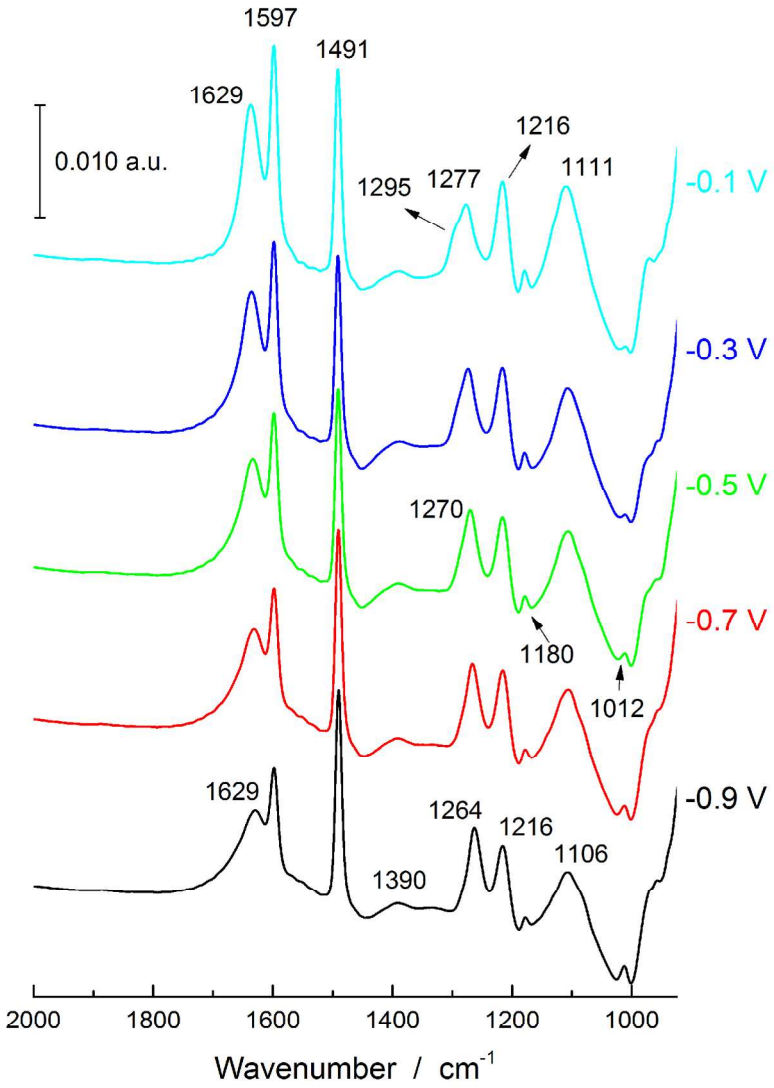

Figure 4. ATR-SEIRA spectra of 4-ABT on nanostructured Cu collected at potentials ranging from -0.9 V (dosing potential) up to -0.10 V.
135x203mm (300 x 300 DPI)

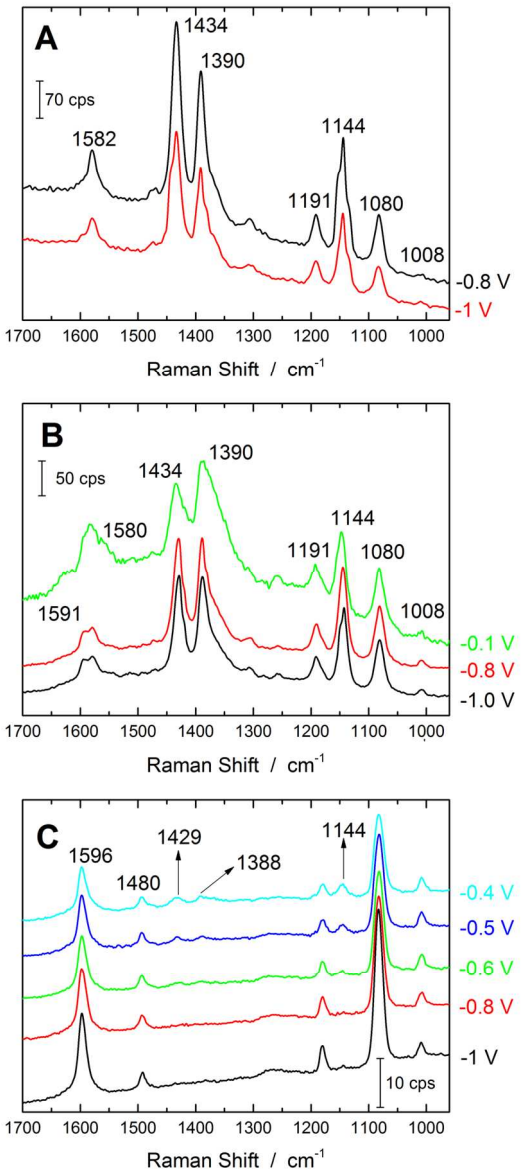

Figure 5. SERS spectra at different potentials of a self-assembled monolayer of 4-ABT from copper surfaces decorated with copper nanostructures, using lasers at 532 nm (acquisition time 10 s) (A), 632.8 nm (acquisition time 30 s) (B) and 785 nm (acquisition time 50 s) (C) as excitation sources. Laser power density about 108 mW cm-2.
80x180mm (300 x 300 DPI)

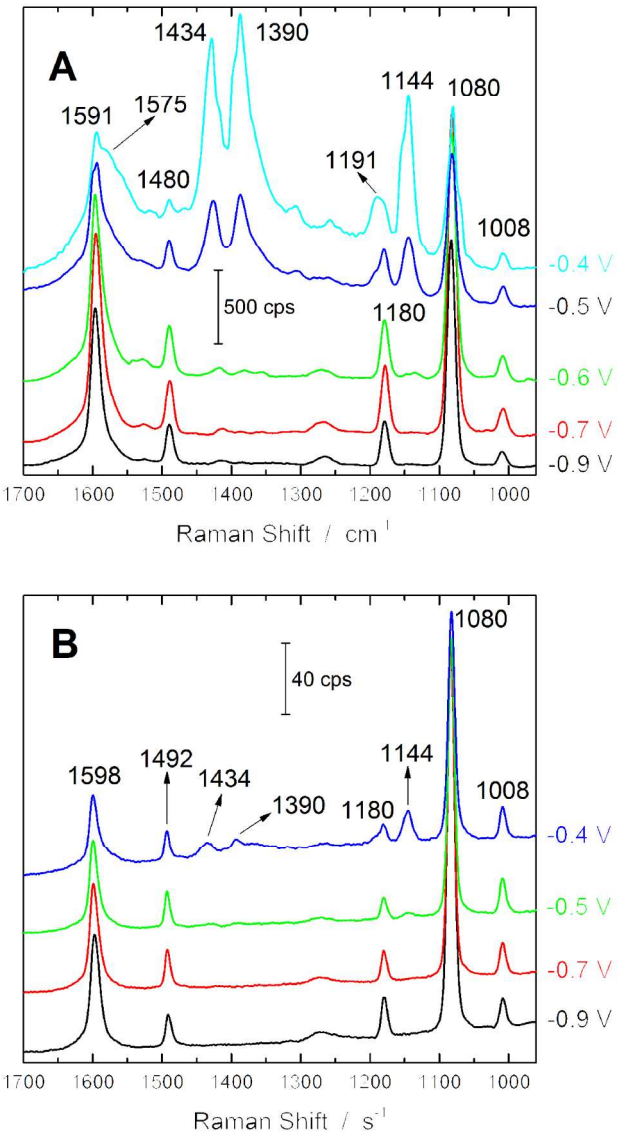

Figure 6. SERS spectra at different potentials of a self-assembled monolayer of 4-ABT from silver surfaces decorated with silver nanostructures using the lasers at 532 nm (A) and 785 nm (B).
108x203mm (300 x 300 DPI)

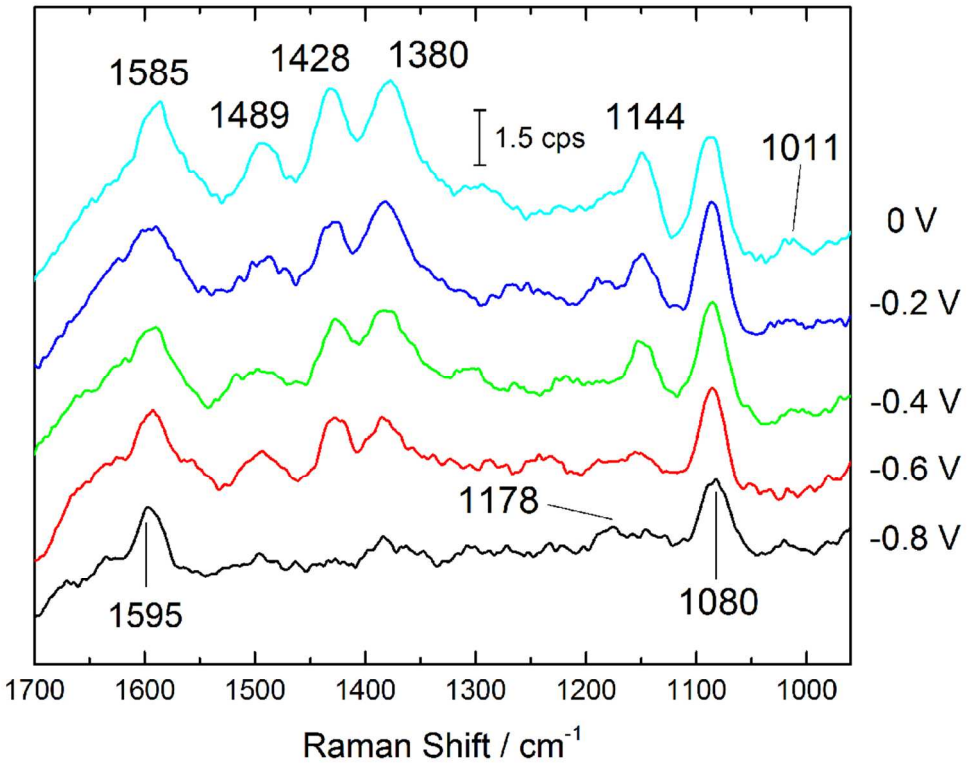

Figure 7. Potential dependent SERS of a self-assembled monolayer of 4-ABT from nanostructured copper surfaces spectra excited by a laser power density about 103 mW.cm-2 of the 632.8 nm laser. Acquisition time 90 s.
99x80mm (300 x 300 DPI)

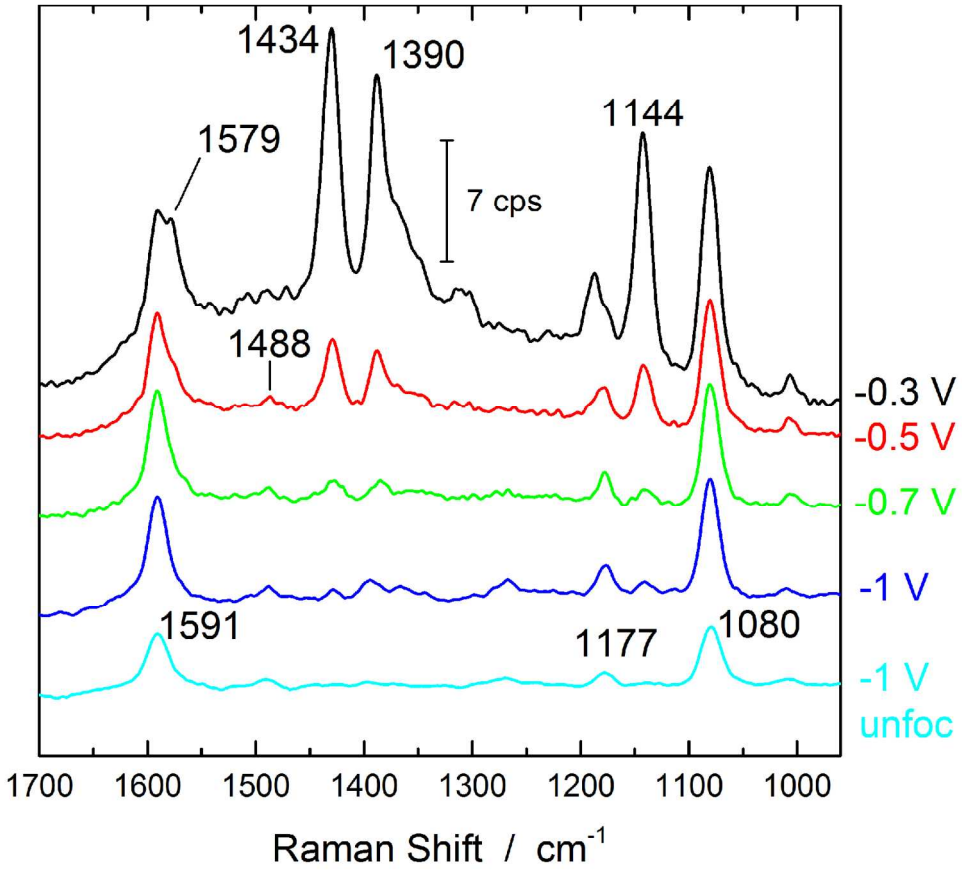

Figure 8. Potential dependent SERS spectra of the 4,4'-DMAB adsorbed on the nanostructured Cu obtained with the laser at 632.8 nm with a power density about 108 mW cm-2. The spectrum at the bottom obtained with the same laser and a power density about 103 mW cm-2.
152x152mm (300 x 300 DPI)

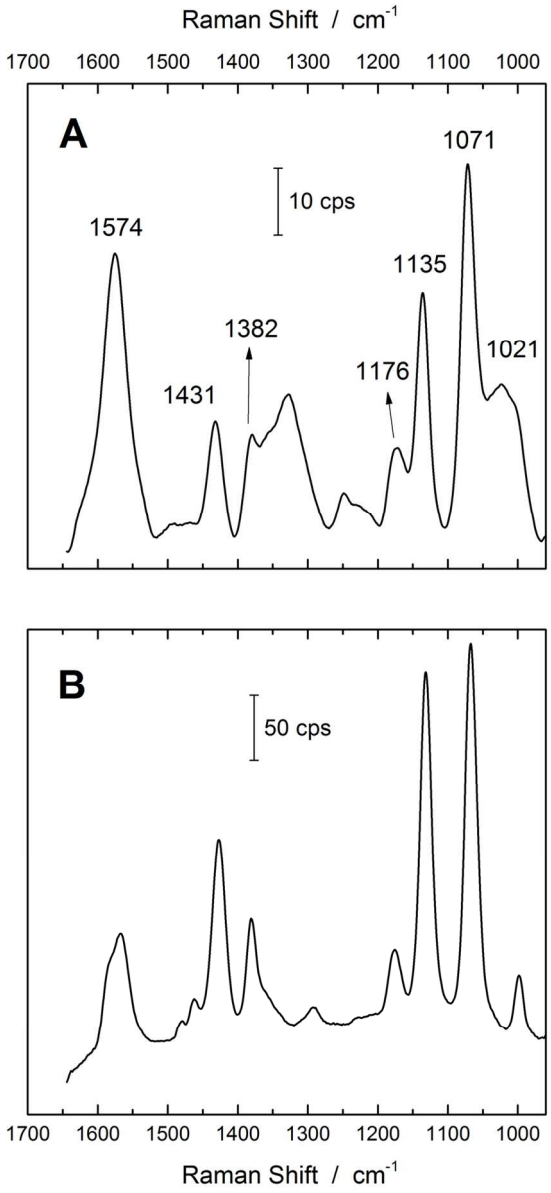

Figure 9. SERS spectra of 4-ABT adsorbed on nanostructured surfaces of Cu (A) and Ag (B) excited by a 1064 nm laser in absence of solution (without control of potential). Laser power density about 109 mW cm-2. Acquisition time 30 s for Cu and 20 s for Ag.
80x167mm (300 x 300 DPI)

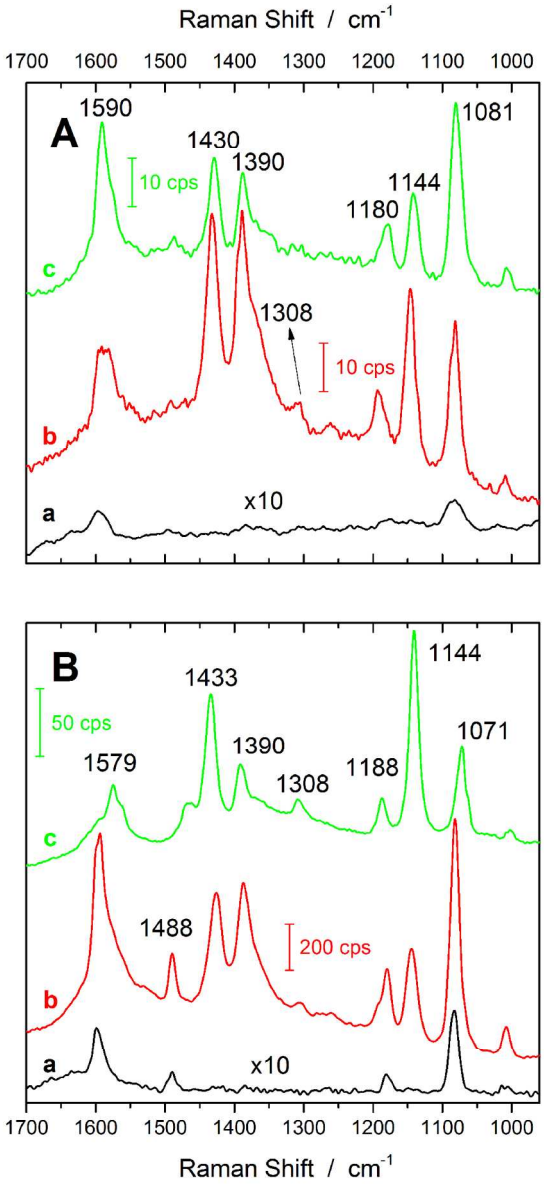

Figure 10. SERS spectra from 4-ABT (a and b) and 4,4'-DMAB (c) adsorbed on Cu (A) and Ag (B) at the same electrode potential (-0.4 V) for which no reduction process takes place with a 632.8 nm laser. Spectra (a) obtained with a power density about 103 mW cm-2. Spectra (b) and (c) obtained with a power density about 108 mW cm-2.
108x203mm (300 x 300 DPI)